*J Physiol* 594.20 (2016) pp 5899–5921



The Journal of Physiology

# Xanthine oxidoreductase mediates membrane docking of milk-fat droplets but is not essential for apocrine lipid secretion

Jenifer Monks[1], Monika Dzieciatkowska[2], Elise S. Bales[1], David J. Orlicky[3], Richard M. Wright[†] and James L. McManaman[1]

[1]*Division of Reproductive Sciences, Department of Obstetrics and Gynecology, School of Medicine, University of Colorado Anschutz Medical Center, Aurora, CO 80045, USA*
[2]*Biochemistry Department, School of Medicine, University of Colorado Anschutz Medical Center, Aurora, CO 80045, USA*
[3]*Department of Pathology, School of Medicine, University of Colorado Anschutz Medical Center, Aurora, CO 80045, USA*

**Key points**

- Xanthine oxidoreductase (XOR) modulates milk lipid secretion and lactation initiation.
- XOR is required for butyrophilin1a1 clustering in the membrane during milk lipid secretion.
- XOR mediates apical membrane reorganization during milk lipid secretion.
- Loss of XOR delays milk fat globule secretion.
- XOR loss alters the proteome of milk fat globules.

**Abstract** Apocrine secretion is utilized by epithelial cells of exocrine glands. These cells bud off membrane-bound particles into the lumen of the gland, losing a portion of the cytoplasm in the secretion product. The lactating mammary gland secretes milk lipid by this mechanism, and xanthine oxidoreductase (XOR) has long been thought to be functionally important. We generated mammary-specific XOR knockout (MGKO) mice, expecting lactation to fail. Histology of the knockout glands showed very large lipid droplets enclosed in the mammary alveolar cells, but milk analysis showed that these large globules were secreted. Butyrophilin, a membrane protein known to bind to XOR, was clustered at the point of contact of the cytoplasmic lipid droplet with the apical plasma membrane, in the wild-type gland but not in the knockout, suggesting that XOR mediates 'docking' to this membrane. Secreted milk fat globules were isolated from mouse milk of wild-type and XOR MGKO dams, and subjected to LC-MS/MS for analysis of protein component. Proteomic results showed that loss of XOR leads to an increase in cytoplasmic, cytoskeletal, Golgi apparatus and lipid metabolism proteins associated with the secreted milk fat globule. Association of XOR with the lipid droplet results in membrane docking and more efficient retention of cytoplasmic components by the secretory cell. Loss of XOR then results in a reversion to a more rudimentary, less efficient, apocrine secretion mechanism, but does not prevent milk fat globule secretion.

(Received 5 March 2016; accepted after revision 14 June 2016; first published online 30 June 2016)
**Corresponding author** J. Monks: 12700 E. 19th Ave, Aurora, CO 80045, USA. Email: jenifer.monks@ucdenver.edu

[†]Deceased.

Data are available via ProteomeXchange with identifier PXD003336.



DOI: 10.1113/JP272390

**Abbreviations** ADPH, adipophilin (a.k.a. Plin2); APM, apical plasma membrane; Atgl, adipose triglyceride lipase (a.k.a. Pnpla2); Btn, butyrophilin1a1; CAD, collision-assisted dissociation; CideA, cell death-inducing DFFA-like effector A; CLD, cytoplasmic lipid droplet; ER, endoplasmic reticulum; FABP, fatty acid binding protein; FFPE, formaldehyde-fixed paraffin-embedded; H&E, haematoxylin and eosin; L10, lactation day 10; LC-MS/MS, liquid chromatography tandem mass spectroscopy; MEC, mammary epithelial cell; MFG, milk fat globule; Mfge8, milk fat globule EGF-like protein/lactadherin; MFGM, milk fat globule membrane; MGKO, mammary gland knockout; NSAF, normalized spectral abundance factor; Plin2, perilipin 2; Pnpla2, patatin-like phospholipase domain-containing protein; RNS, reactive nitrogen species; ROS, reactive oxygen species; WT, wild-type; XDH, xanthine dehydrogenase; XOR, xanthine oxidoreductase.

## Introduction

Lactation, or milk secretion, evolved in mammals to provide nutrition and immune protection to the young. The lactating mammary gland is considered a classical exocrine gland. Secretion of milk components by the mammary epithelial cell utilizes five discrete cellular pathways, including (1) exocytosis of milk proteins and lactose, (2) transcytosis of serum proteins, (3) membrane transporters for small molecules, (4) a regulated paracellular pathway and (5) an apocrine secretion pathway for milk lipids (McManaman & Neville, 2003). Apocrine secretion of milk lipids is fundamentally distinct from the exocytotic mechanisms used for secretion of lipids into serum and lymph (McManaman, 2012). Milk lipids originate by direct membrane envelopment of cytoplasmic lipid droplets (CLDs) at the apical plasma membrane (APM), releasing membrane-bound particles (referred to as milk fat globules – MFGs) containing intact CLDs and elements of the cytoplasm into the lumen of the gland (Mather & Keenan, 1998). Although there is general consensus that milk lipids are secreted by a membrane envelopment process, details about the molecular machinery mediating this secretion are limited and remain controversial (McManaman, 2012; Heid and Keenan, 2005; Jeong *et al.* 2013).

Xanthine oxidoreductase (XOR) is an enzyme originally isolated from bovine milk and is very abundant in milk fat (reviewed by Harrison, 2006). It is a large, well-conserved, metalloenzyme that regulates purine breakdown within the cell. It exists in two, enzymatically distinct forms, a dehydrogenase form, which passes reducing equivalents to $NAD^+$ and an oxidase form which passes them to molecular oxygen, nitrate or nitric oxide and generates reactive oxygen or nitrogen species (ROS or RNS). The dehydrogenase form predominates within the mammary secretory cell, but the oxidase form is found in milk (McManaman *et al.* 2002). XOR has long been thought to be a scaffolding protein, essential for secretion of milk lipids, adjoining the lipid droplet coat protein, perilipin2/adipophilin (Plin2/ADPH), and the integral membrane protein, butyrophilin (Btn). XOR has been shown to bind directly to a specific C-terminal domain of Btn (Ishii *et al.* 1995; Jeong *et al.* 2009), to be covalently bound within a larger complex with Btn and Plin2 (McManaman *et al.* 2002), and its housekeeping enzyme function is not thought to be necessary for this process. Rather, XOR is thought to have been borrowed by evolution to enhance the efficiency of nutrient delivery to the neonate (Oftedal, 2012). Here we tested this conclusion directly by deleting XOR from the mammary epithelial cell and measuring the efficiency of lactation.

As whole body XOR deletion is lethal in mice before reproductive maturity (Vorbach *et al.* 2002; Ohtsubo *et al.* 2009), we used the Cre–Lox system for conditional deletion of XOR in the mammary epithelial cells. XOR f/f animals have exons 3 and 4 flanked by LoxP sites, which generates a premature stop codon when recombined by the Cre-recombinase (Fini *et al.* 2014, 2016). Breeding these animals to the previously described BLG-Cre mouse (Selbert *et al.* 1998) allowed deletion of the XOR specifically in the milk-secreting cells, during late pregnancy. We hypothesized that lactation would fail in these animals due to an inability to secrete milk fat as has previously been reported in XOR-deficient mice, CideA-knockout mice and Btn-knockout mice (Vorbach *et al.* 2002; Ogg *et al.* 2004; Wang *et al.* 2012). Surprisingly, the pups survived and MFGs were secreted, hinting at a possible compensatory secretion mechanism. Since milk secretion did not fail catastrophically in mice lacking XOR in their mammary glands (MGKO), we used this novel model to investigate the cellular mechanism of milk lipid secretion and define the precise role of XOR in this process.

To define the proteins mediating their secretion, we floated and washed MFGs from the XOR dams and subjected them to proteomic analysis. We used label-free counting of the peptide spectra to show quantitative differences in the protein components of the globules from XOR knockout and wild-type littermates. We saw changes in the proteome of the globules that suggested differences in the secretory mechanism itself, notably an increase in many proteins that are usually retained within the cell in the wild-type dams. Although the proteome of the mouse MFG has been previously published (Wu *et al.* 2000), this study utilized a more modern approach and identified 25-fold more proteins. Additionally, other groups have published the MFG proteomes for major dairy species and for humans (Affolter *et al.* 2010; Liao *et al.* 2011; Picariello *et al.* 2012; Spertino *et al.* 2012). To our knowledge, this is the first use of proteomics technology to discern changes

in secretory mechanisms following knockout of a specific mediator of apocrine secretion.

## Methods

### Ethical approval

We understand the ethical principles under which the *Journal of Physiology* operates and confirm that our work complies with the published animal ethics checklist. Animals were humanely treated and killed in accordance with the Guide for Care and Use of Laboratory Animals (8th edn), by personnel trained in their care. All procedures were approved by the Institutional Animal Care and Use Committee of the University of Colorado Denver Anschutz Medical Campus, on protocol B79213(11)1E.

### Animal care

Mice were house in the University of Colorado Denver Anschutz Medical Campus, AAALAC-accredited, Centre for Comparative Medicine. Mice had *ad libitum* access to food (Harlan 2920x), in micro-isolator cages with automated air and water, on a 10:14 h dark/light cycle, maintained at 72°F. All animals were provided with cotton nesting material enrichment and breeders and experimental females were additionally provided with shredded paper to construct an enclosed nest.

$XOR^{f/f}$ mice (created by R.M.W.) were bred with three strains to delete XDH/XOR from the milk-secreting, mammary alveolar cells: (1) MMTV-Cre [Jackson Labs no. 003553, STOCK Tg(MMTV-cre)4Mam/J], (2) BLG-Cre mice (a kind gift of Trevor Williams, University of Colorado, now available at Jackson Laboratories) and (3) WAP-Cre (a gift of Kay-Uwe Wagner, University of Nebraska Medical Centre) to create the XOR MGKO lines. Histological analysis of hemizygous knockout animals was performed to verify that Cre expression was not deleterious. Otherwise, Cre-negative littermates were used as controls for all experiments.

### Induction of pregnancy and lactation

Experimental females age 8–16 weeks were placed with proven C57Bl/6 stud males. The presence of a vaginal plug was recorded and counted as pregnancy day 1. Dams were individually housed prior to parturition. The day a litter was first seen was counted as lactation day 0 (L0). Litters were standardized to eight pups by culling or cross-fostering. Culled neonatal animals were humanely killed using $CO_2$ followed by decapitation. Dam and litter weights were collected throughout lactation and tissue was weighed and collected after the animals had been killed. Dams and pups older than 10 days were killed by $CO_2$ followed by cervical dislocation. No differences were noted with increasing parity of the dams.

### Milk collection

Pups were removed from dams for 3 h to allow milk accumulation in the mammary glands. Milk removal was essentially as described (DePeters & Hovey, 2009, Method 2) except that xylazine alone was used as a sedative and muscle relaxant. Briefly, xylazine was given I.P. at a dose of 8 mg $kg^{-1}$. When the mouse was relaxed enough to have ceased ambulation around the cage (about 5 min), the milking procedure was begun. The mouse was picked up, and with gentle hand-restraint, a single dose of oxytocin (0.5 IU, 0.25 ml in sterile saline) was given I.P. Milk let-down occurred within 1 min and milk removal was started. Our standard milking apparatus, attached to house vacuum, was used. Standard hand restraint was used throughout the milking procedure.

Milk was collected and processed at room temperature to avoid changes in protein segregation between phases (Dickow *et al.* 2011). Gentle inversion to homogenize the milk sample was performed immediately prior to crematocrit sampling. Ten microlitres of whole milk was loaded into Drummond Microcap haematocrit tubes that were then sealed with Hemato-seal (Fisher Scientific, Houston, TX, USA). The tubes were centrifuged at 1500***g*** at room temperature to float the cream. The lipid fraction was measured linearly across the tube and divided by the length of the total milk column to give the fat percentage (Lucas *et al.* 1978). To isolate the MFGs, whole milk was mixed 1:1 with 10% sucrose and layered under 10+ ml of PBS. This preparation was centrifuged at 1500 *g* at room temperature. The floated globules were collected, washed with PBS twice more and stored at −80°C until further analysed.

### Proteomic analysis: sample preparation

The MFG proteins were prepared essentially as previously published (Wisniewski *et al.* 2009), from the milk of four wild-type and four XOR MGKO dams (L10). Briefly, isolated MFGs were precipitated with 10% trichloroacetic acid for 2 h at −20°C. The precipitated protein samples were pelleted by centrifugation at 14,000 *g* for 20 min at 4°C, rinsed in ice-cold acetone and centrifuged again. The pellet was air-dried and solubilized in 4% SDS, 100 mM DTT in 100 mM Tris-HCI, pH 7.5. Sample was incubated for 10 min at 90°C, centrifuged at 14,000 *g* for 10 min and the floating cream layer was removed. The protein concentrations were determined by the BCA Protein Assay. Proteins were digested according to the FASP protocol using a 30 kDa molecular weight cutoff filter. In brief, samples were mixed in the filter unit within 8 M urea in 0.1 M Tris-HCl, pH 8.5, and centrifuged at 14,000 *g* for

15 min. The proteins were reduced by addition of 100 $\mu$l of 10 mM DTT in 8 M urea in 0.1 M Tris-HCl, pH 8.5, with incubation for 30 min at room temperature and the device was centrifuged. Subsequently, 100 $\mu$l of 55 mM iodoacetamide in 8 M urea in 0.1 M Tris-HCl, pH 8.5, was added to the samples, with incubation for 30 min at room temperature in the dark followed by centrifugation. Afterward, three washing steps with 100 $\mu$l of 8 M urea in 0.1 M Tris-HCl, pH 8.5, solution were performed, followed by three washing steps with 100 $\mu$l of 50 mM ABC buffer. Proteins were digested with trypsin overnight at 37°C. Peptides were recovered from the filter using 30% acetonitrile. The volume of the eluted sample was reduced to ~2 $\mu$l in a vacuum centrifuge and reconstituted to 50 $\mu$l with 0.1% formic acid.

### LC–MS/MS analysis

Samples were analysed on an LTQ Orbitrap Velos mass spectrometer (Thermo Fisher Scientific) coupled to an Eksigent nanoLC-2D system through a nanoelectrospray LC−MS interface. A sample volume of 8 $\mu$l was injected into a 10 $\mu$l loop using the autosampler. To desalt the sample, material was flushed out of the loop and loaded onto a trapping column (ZORBAX 300SB-C18, dimensions 5×0.3 mm, 5 $\mu$m) and washed with 0.1% formic acid at a flow rate of 5 $\mu$l min$^{-1}$ for 5 min. The analytical column was then switched on-line at 600 nl min$^{-1}$ over an in-house 100 $\mu$m i.d. × 200 mm fused silica capillary packed with 4 $\mu$m 80Å Synergi Hydro C18 resin (Phenomex; Torrance, CA, USA). After 10 min of sample loading, the flow rate was adjusted to 350 nl min$^{-1}$, and each sample was run on a 120 min linear gradient of 5–40% acetonitrile with 0.1% formic acid to separate the peptides. LC mobile phase solvents and sample dilutions used 0.1% formic acid in water (Buffer A) and 0.1% formic acid in acetonitrile (Buffer B) (Chromasolv LC–MS grade; Sigma-Aldrich, St. Louis, MO, USA). Data acquisition was performed using the instrument-supplied Xcalibur (version 2.1) software. The mass spectrometer was operated in positive ion mode. Each survey scan of *m/z* 400–2000 was followed by collision-assisted dissociation (CAD) MS/MS of 20 most intense precursor ions. Singly charged ions were excluded from CAD selection. Normalized collision energies were employed using helium as the collision gas. Each sample was analysed in duplicate.

### Database searching, protein identification

MS/MS spectra were extracted from raw data files and converted into mgf files using a PAVA script (UCSF, MSF, San Francisco, CA, USA). These mgf files were then independently searched against the mouse SwissProt database using an in-house Mascot server (Version 2.2.06, Matrix Science, London, UK). Mass tolerances were ±15 p.p.m. for MS peaks, and ±0.6 Da for MS/MS fragment ions. Trypsin specificity was used allowing for one missed cleavage. Met oxidation, protein N-terminal acetylation, peptide N-terminal pyroglutamic acid formation, deamidation of asparagine, glutamine and tryptophan, sulphone of methionine, and tryptophan oxidation to formylkynurenin of tryptophan were allowed for variable modifications while carbamidomethyl of Cys was set as a fixed modification. The MS proteomics data have been deposited to the ProteomeXchange Consortium (Vizcaíno *et al.* 2014) via the PRIDE partner repository with the dataset identifier PXD003336 and 10.6019/PXD003336.

Scaffold (version 4.3.2, Proteome Software, Portland, OR, USA) was used to validate MS/MS-based peptide and protein identifications. Peptide identifications were accepted if they could be established at greater than 95.0% probability as specified by the Peptide Prophet algorithm. Protein identifications were accepted if they could be established at greater than 99.0% probability and contained at least two identified unique peptides in the first set of experiments.

### Immunofluorescence staining and imaging

Formaldehyde-fixed, paraffin-embedded tissue was sectioned by the Histology Core facility. Sections of 5 $\mu$m were stained with haematoxylin and eosin (H&E) and histological images were captured on an Olympus BX51 microscope equipped with a 4 Mpixel Macrofire digital camera (Optronics, Goleta, CA, USA) using the PictureFrame Application 2.3 (Optronics). All images were cropped and assembled using Photoshop CS2 (Adobe Systems, Mountain View, CA, USA). For immunostaining, sections were deparaffined with xylene and graded ethanols and antigen retrieval was performed using a citrate-based solution (VectorLabs, Burlingame, CA, USA). The sections were permeabilized with saponin and glycine, and blocked with 10% donkey serum. Stains included: guinea pig anti-Plin2 (1:200, Fitzgerald, Acton, MA, USA), guinea pig anti-butyrophilin (1:200, Progen Biotechnik GmbH, Heidelberg, Germany), rabbit anti-CideA (1:100, AbD Serotec/Bio-Rad, Raleigh, NC, USA), wheat germ agglutinin (Alexa 555 conjugate, Invitrogen, Carlsbad, CA, USA), and DAPI (Sigma, D9542). Secondary antibodies were from Jackson ImmunoResearch (West Grove, PA, USA). Sections were mounted with ProLong Gold (Molecular Probes, Eugene, OR, USA). MFG staining was performed on freshly isolated, never-frozen milk samples, using BODIPY 493/503 (Invitrogen), and imaged neat. For analysis of cytoplasmic crescents, whole milk was mixed with LipidTox Red and Alexa 488-phalloidin (Invitrogen, Carlsbad, CA, USA). Imaging was performed on a Marianas Spinning Disc

confocal microscope (Intelligent Imaging Innovations, Inc., Denver, CO, USA), using a 100× objective (plan apochromat, NA 1.4). Analysis was performed using SlideBook v. 6.0 (Intelligent Imaging Innovations), on 10–20 images from at least three animals per group.

### EM analysis

Dams with standardized litters were killed by $CO_2$ and immediately perfused, intra-cardiac, with PBS, then 2 and 4% paraformaldehyde. Dissected glands were post-fixed in specialized EM fixative (2.5% glutaraldehyde, 1% acrolein, 20 mM $MgCl_2$ in 0.1 M phosphate, pH 7.4), and then in 2% $OsO_4$ in phosphate buffer. Tissues were dehydrated in a graded series of ethanol, and infused with propylene oxide/resin 3:1, propylene oxide/resin 1:1 overnight, and fresh pure resin for 8 h, then final resin overnight at 60°C. Resin-embedded samples were sectioned at 60 nm and collected on 200 mesh copper grids. Sections were post-stained with 2% uranyl acetate and Reynold's lead citrate. Transmission electron microscopy images were collected on a FEI Technai microscope, using a Gatan UltraLight digital camera system.

### Statistical analysis

Statistical analysis was performed using the software Prism 6 from GraphPad Software (La Jolla, CA, USA).

## Results

### XOR modulates milk lipid secretion and lactation initiation

Conditional deletion of XOR in the milk-secreting, mammary alveolar cell was achieved by crossing floxed XOR mice with the three most common mammary-specific Cre-expressing lines: mouse mammary tumor virus (MMTV)-Cre (Wagner *et al.* 2001), whey acidic protein (WAP)-Cre (Wagner *et al.* 1997) and beta-lactoglobulin (BLG)-Cre (Selbert *et al.* 1998). Dams from all three crosses produce viable offspring and nurse to weaning. All three lines exhibit some degree of litter growth restriction compared to wild-type (WT) dams, and their mammary glands have similar histological phenotypes at mid-lactation characterized by many large CLDs trapped inside alveolar epithelial cells (Fig. 1*A*, asterisks). Conditional deletion using the BLG-Cre model shows the least mosaicism and, surprisingly, the least growth restriction (data not shown) and so this model was chosen for further analysis.

Growth rates of standardized litters are traditionally used to measure milk secretion rates in genetically modified mice. Dams were impregnated by WT males and, following parturition, litters were standardized to eight pups and were weighed daily for the duration of lactation. Litter weights of hemizygous and homozygous XOR MGKO dams on L1 and L2 are markedly reduced compared to WT dams, suggesting that loss of a single copy of XOR in mammary glands of mice is sufficient to delay lactation initiation (Fig. 1*B*, *C*). We did not detect differences in litter growth rates between the WT and hemizygous MGKO mice at later stages of lactation, although growth of litters nursing the homozygous MGKO dams was reduced from 3.2 to 2.6 g $day^{-1}$ (Fig. 1*B*–*E*). To verify that mammary development during pregnancy is not compromised by XOR loss, we compared the histology of mammary glands of dams at late pregnancy. At pregnancy day 18, mammary glands of MGKO mice show no difference in gross weight, adipocyte component, alveolar outgrowth or differentiated phenotype as evidenced by secretory product within the lumen, and CLD accumulation (data not shown).

### XOR mediates docking of the CLDs to the apical plasma membrane

Histological analyses of the mammary gland at mid-lactation (L10) were used define the effects of XOR deletion. Figure 1*A* shows that mammary glands of MGKO dams contain many, very large CLDs within the mammary epithelial cells, often reaching from the basal to the apical side of the mammary epithelial cell. Examining these glands under the electron microscope (Fig. 2), we see that CLDs in WT mammary epithelial cells appear to be closely associated with the apical border of the cell, as previously described (Heid & Keenan, 2005) Microvilli are lost in this region and no organelles or cytoplasmic contents are seen between the CLDs and the membrane. In contrast, CLDs in the XOR MGKO appear to be separated from the apical border of the cell by a thin layer of cytoplasm (Fig. 2*F*, arrowheads), suggesting that XOR may be required for close association, or 'docking', of CLDs with the APM during milk lipid secretion.

### XOR draws Btn into the membrane domain where CLDs are docked

XOR is hypothesized to induce CLD–membrane docking sites by binding to the integral membrane protein, Btn, and inducing its oligomerization (Mather and Keenan, 1998; Jeong *et al.* 2013). We formally tested this hypothesis by immunostaining formaldehyde-fixed, paraffin-embedded (FFPE) tissue from day 10 lactating WT and XOR MGKO dams, with antibodies against Plin2 and Btn. In both WT and MGKO dams, Plin2 exclusively localizes to the surface of CLDs and Btn staining is found at the APM, as well as in secretory vesicles as previously reported (Russell *et al.* 2007; Wooding *et al.* 2015) (Fig. 3*A*). However,

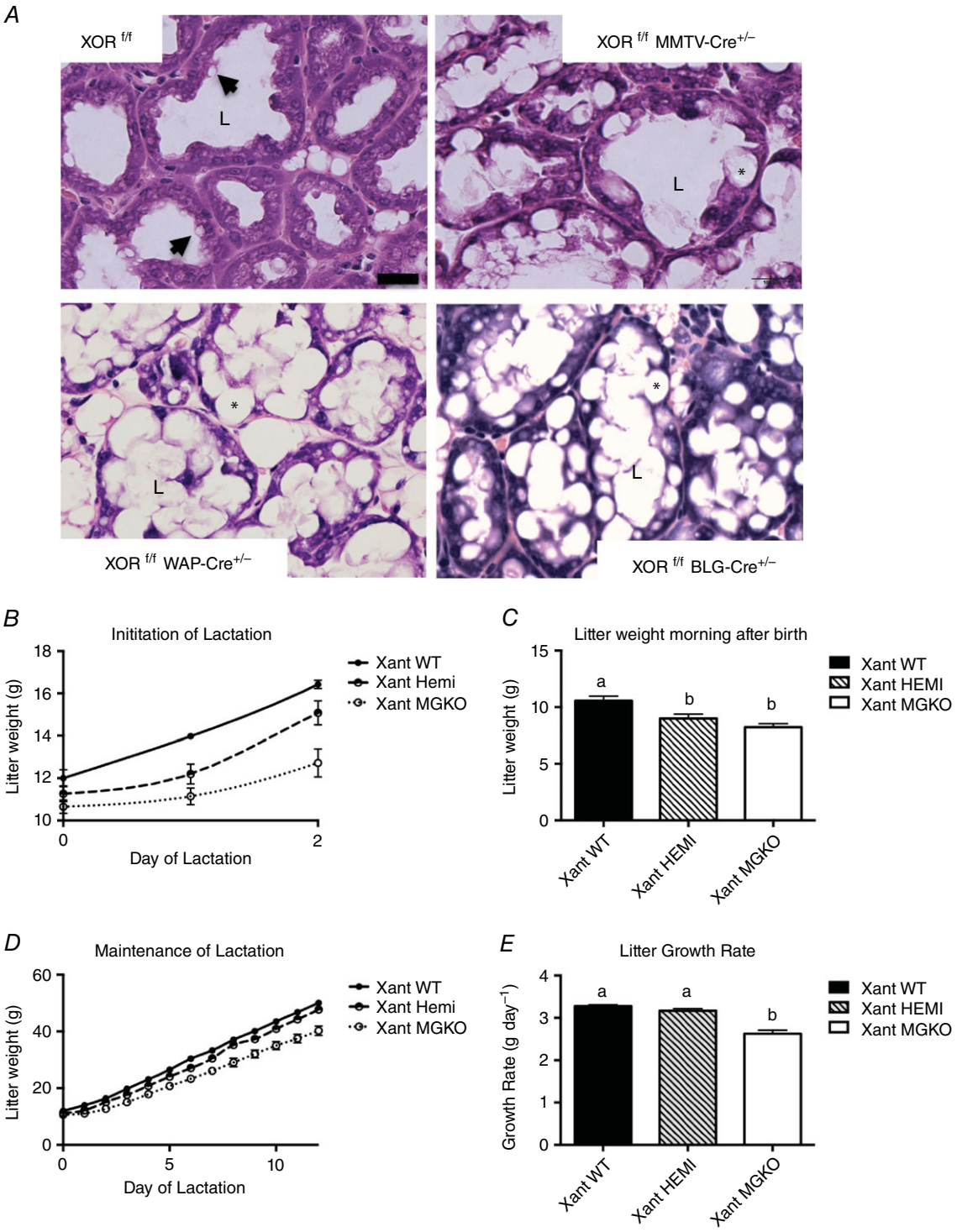


**Figure 1. Conditional knockout models of XOR in the mammary gland show a modest lactation defect**
*A*, H&E-stained FFPE tissue from dams at lactation day 10–12 with the following genotypes: $XOR^{flox/flox}$, $XOR^{flox/flox}$, MMTV-$Cre^{+/-}$, $XOR^{flox/flox}$, WAP-$Cre^{+/-}$ and $XOR^{flox/flox}$, BLG-$Cre^{+/-}$. Luminal spaces are marked with an L. Arrows indicate small lipid droplets docked at the apical plasma membrane (APM) of the mammary epithelial cell (MEC). Asterisks indicate large lipid droplets within the MEC in the XOR MGKO glands. Bar = 100 $\mu$m. *B*, litter growth curves for lactation days 0–2 shown for $XOR^{flox/flox}$ (WT) dams, $XOR^{flox/+}$, BLG-$Cre^{+/-}$ (HEMI) dams and $XOR^{flox/flox}$, BLG-$Cre^{+/-}$ (MGKO) dams. *C*, litter weights for eight pups, the morning after birth. ($^{a,b}P<0.05$). *D*, litter growth curves for lactation days 0–12 for the same groups. *E*, litter growth rates for days 3–12 for the above groups ($^{a,b}P<0.005$). [Colour figure can be viewed at wileyonlinelibrary.com]

in mammary glands of WT dams, Btn staining intensity is markedly increased at CLD–membrane docking sites (Fig. 3*A*, arrowheads). Image analysis (Fig. 3*B*) shows that the average distance between peak Plin2 and Btn immunofluorescence is significantly greater in MGKO than in WT mice, which supports electron microscopy data showing that CLDs in mammary glands of MGKO mice do not exhibit the same close membrane association as they do in WT mice. Collectively, these data are consistent with the hypothesized role of XOR in mediating Btn oligomerization and suggest that XOR–Btn interactions induce apical membrane alterations involved in CLD docking.

To test the hypothesis that XOR–Btn interactions alter apical membrane properties at sites of CLD secretion, we investigated the effects of XOR deletion on the surface distribution of apical membrane-enriched glycoproteins using the fluorescently labelled lectin, wheat germ agglutinin (WGA). In mammary glands of WT mice, apical membrane regions enriched in Btn staining are relatively depleted of WGA staining compared to membrane regions adjacent to these sites (Fig. 3*C*, Movies 1, 2). To determine if decreased WGA levels at CLD docking sites correspond to enrichments in Btn we next mapped spatial relationships between WGA and Btn immunofluorescence intensities on apical membrane regions of WT and MGKO mammary glands. Figure 3*D* shows that in membrane regions surrounding docked CLDs, WGA and Btn fluorescence intensities exhibit anti-correlation, with a Pearson's correlation coefficient of $-0.35 \pm -0.04$. In contrast, in mammary glands of MGKO mice, fluorescence intensities of WGA and Btn are uncorrelated, with an average Pearson's correlation coefficient of $0.13 \pm 0.13$, which is significantly different from WT glands ($P = 0.0004$). This result suggests Btn is drawn from a larger pool in the membrane into the dock by the presence of XOR and that WGA is excluded from this region.

## Docking of CLD to the membrane disassembles the microvilli and remodels the glycocalyx

Changes in the membrane of developing drosophila embryos have been visualized by staining with fluorescently labelled WGA (Figard & Sokac, 2014). We compare WGA fluorescence at APM regions associated with docked and undocked CLDs in secretory epithelial cells of lactating WT and MGKO mice, respectively, using

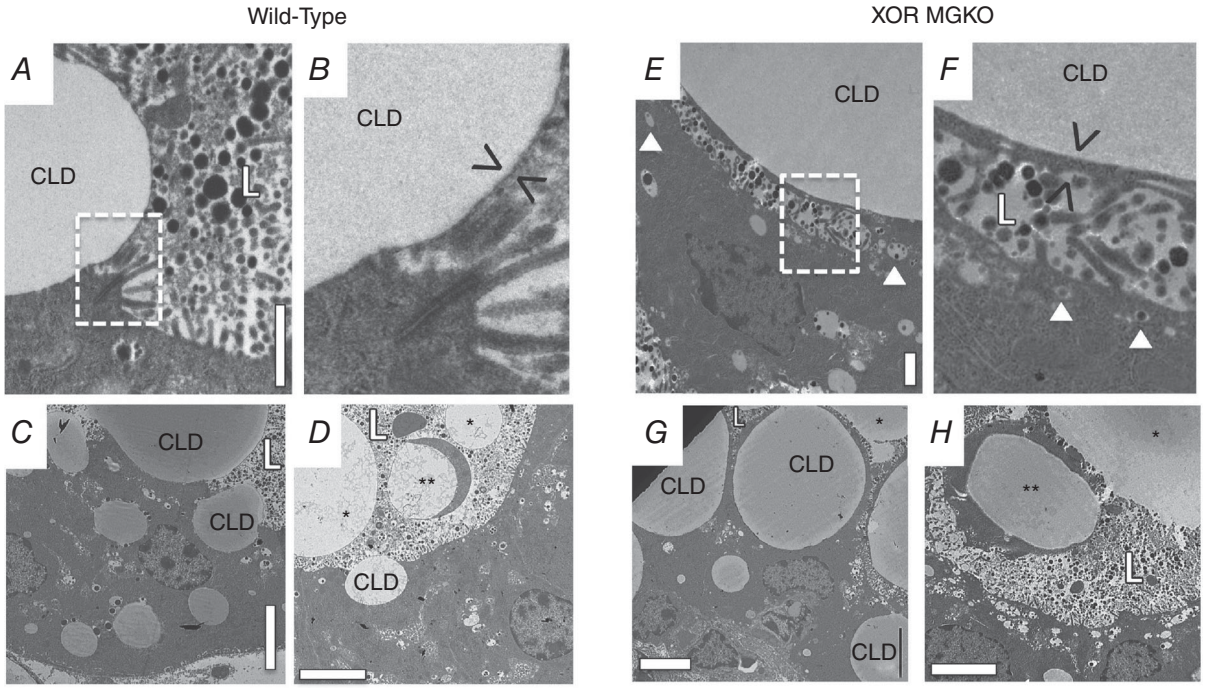


**Figure 2. XOR mediates close association between the cytoplasmic lipid droplet and the apical plasma membrane**
Electron micrographs of lactating mammary gland from WT (*A–D*) and MGKO (*E–H*) dams. *A* and *D*, a cytoplasmic lipid droplet (CLD) near the apical plasma membrane (APM). Bar = 1 $\mu$m. *B* and *F*, enlargement of inset delineated with dotted line. *C* and *G*, alveolar cell with several CLDs near at APM. Bar = 5 $\mu$m. *D* and *H*, secreted MFGs in lumen with attached crescent. Bar = 5 $\mu$m. The luminal space is marked with an L. Arrows delineate distance from CLD to plasma membrane. White arrowheads indicate secretory vesicles containing casein micelles. Secreted MFGs are labelled with an asterisk (*). Those with crescents are marked with double asterisks (**).

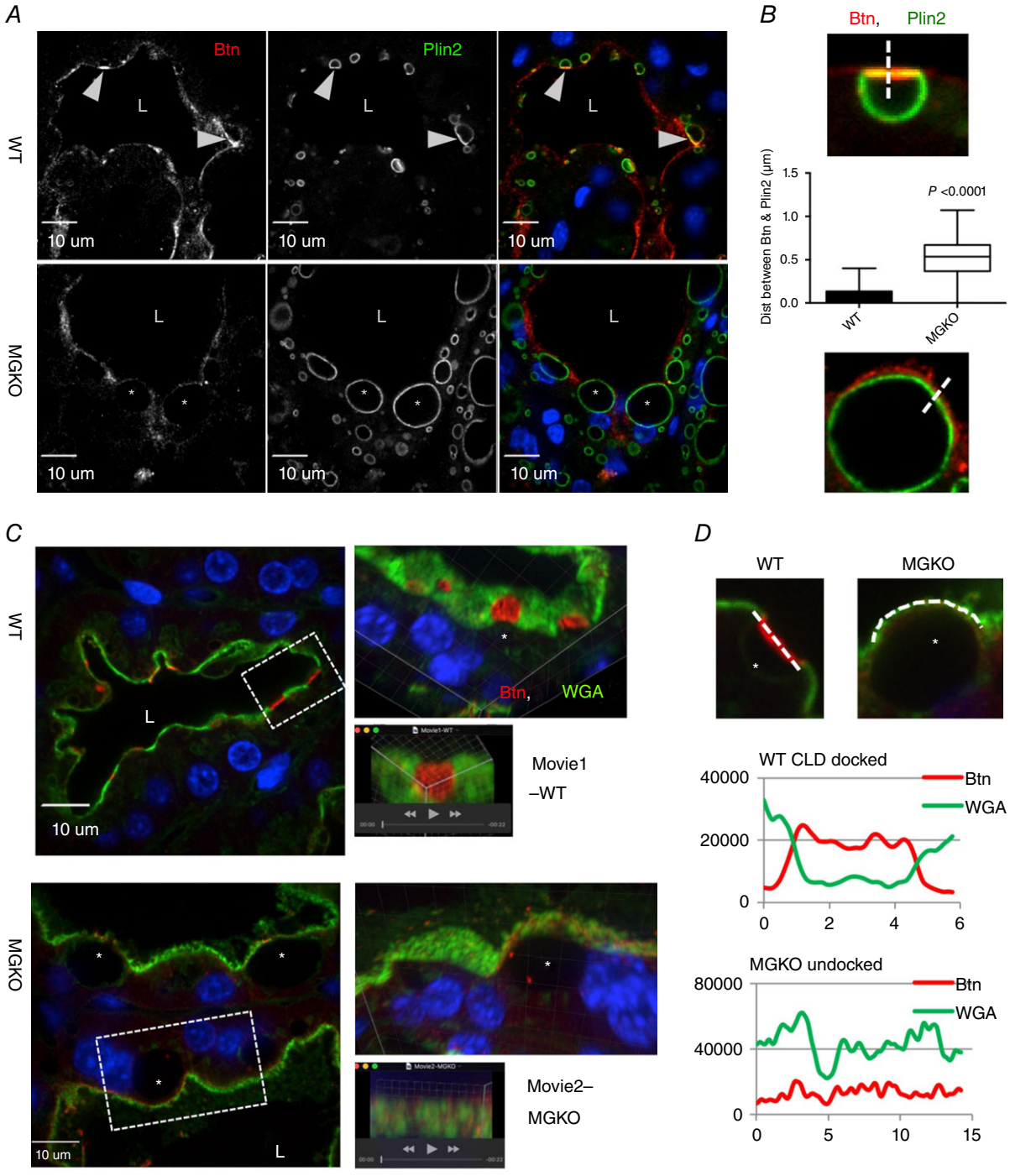


**Figure 3. XOR draws Btn into the membrane domain where CLDs are docked**
*A*, L10 mammary gland from WT and XOR MGKO dams immunostained for Btn (right, and red), Plin2 (middle, and green) and overlay with DAPI (blue). Arrows indicate docked CLDs in the WT gland. Asterisks indicate large CLDs within MGKO glands. Bar = 10 $\mu$m. *B*, line intensity analysis of CLD docking showing peak-to-peak distance between Btn and Plin2 at the membrane (>50 CLD per mouse, three mice per group, $P<0.0001$). *C*, L10 mammary gland from WT and XOR MGKO dams stained with anti-Btn (red), WGA (green) and DAPI (blue), showing Btn (red) staining is clustered in the WT membrane (WGA, green) but not in the MGKO membrane. Bar = 10 $\mu$m. Dotted line indicates enlarged region shown as a 3D projection. Movies show 3D imaging of CLD docking sites in WT and MKGO glands. *D*, line intensity analysis of CLD docking showing segregation of Btn from WGA staining. Pearson's correlation coefficient shows anti-correlation of Btn and WGA in the docked CLD in WT glands ($-0.35 \pm 0.4$) but not in the XOR MGKO glands ($0.13 \pm 0.13$, $P = 0.0004$). Fifty CLDs per group were scored from three animals per group.

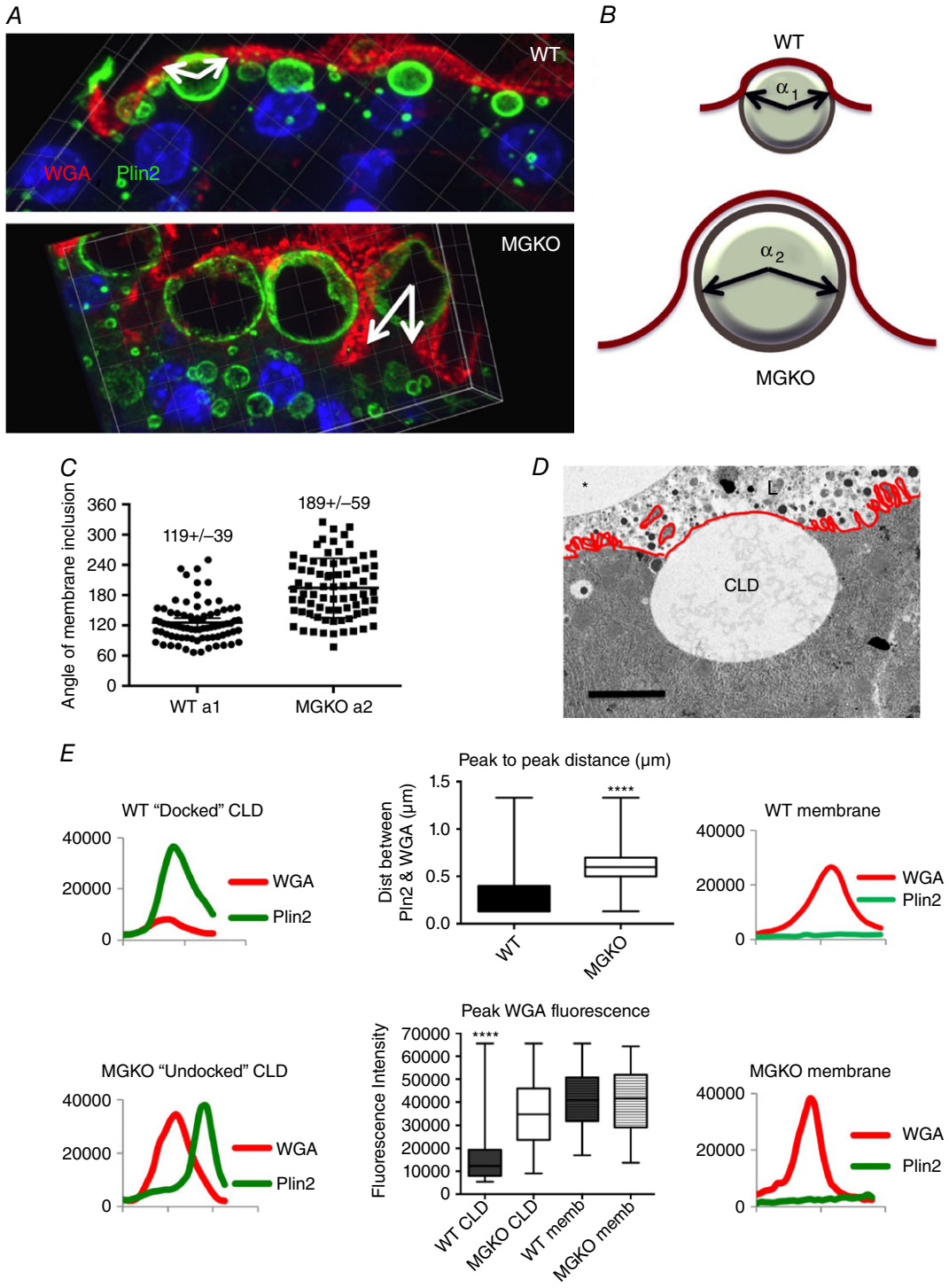


**Figure 4. Docking of CLDs to the membrane disassembles the microvilli and remodels the glycocalyx**
*A*, 3D projections of CLDs at the apical plasma membrane (APM) of WT and MGKO glands, stained with anti-Plin2 (green), WGA (red) and DAPI (blue). Arrows indicate the angle of membrane inclusion. *B*, diagram of angle of inclusion measurements performed on docked CLDs. *C*, angle of inclusion measured in CLDs docked at the APM of WT and MGKO mammary glands (combined data from three mice per group, >50 CLDs per mouse). *D*, electron micrograph of a docked CLD in a WT gland with the membrane colourized (red) to show microvilli and membrane stretch. The luminal space is marked 'L' and a secreted MFG in the lumen is marked with an asterisk. *E*, line intensity analysis of CLDs on Plin2/WGA-stained mammary glands. Peak-to-peak distance is increased with XOR loss. WGA staining of the membrane over the docked CLD is decreased in the WT but not the MGKO gland (>50 CLDs per mouse, three mice per group, $P<0.0001$).

Plin2 immunofluorescence to localize CLDs (Fig. 4*A*). Similar to the electron micrographs previously collected (Fig. 2), in XOR MGKO mammary glands, we notice an expansion of the lumen surrounding the CLDs, apparently created by continued fusion of exocytotic vesicles containing milk proteins (Fig. 2, white arrowheads), similar to a kiss-and-coat mechanism of sequential exocytosis (Sokac & Bement, 2006). Apical membrane extension around large, apically localized CLDs can also be seen in Plin2/WGA-stained MGKO glands (Fig. 4*A*). In some instances, the membrane can be seen to almost completely engulf CLDs in MGKO glands. In contrast, only limited membrane invagination is observed in WT glands. These differences were quantified by determining the angle of CLD inclusion (Fig. 4*B*, *C*). The median angle of CLD inclusion of docked CLDs in WT glands is 119 (±39) deg, with only a few CLDs having an angle of inclusion greater than 180 deg. However, the median angle of CLD inclusion in MGKO mice, 189 (±59) deg, is significantly larger ($P < 0.0001$). Many CLDs in MGKO glands have an angle of inclusion of greater than 240 deg, which is consistent with their nearly complete membrane engulfment prior to secretion. In the case of the mouse mammary gland, membrane derived from exocytotic vesicles is thought to contribute to the final membrane surrounding the secreted MFGs (Kralj *et al.* 1992, Wooding *et al.* 2015). Similarly, in the XOR MGKO gland, continued exocytosis appears to contribute to membrane invagination of large CLDs, possibly mediating their secretion.

Figure 4*D* shows an electron micrograph of a docked CLD in a WT gland, with the apical border highlighted in red, showing that the microvilli are lost/disassembled in the docking region. Using the measured angle of inclusion, we calculated the amount of additional membrane contained in the microvilli to account for the additional stretch. If the range is 80–158 deg, then the APM must stretch 33–68%, to create the spherical cap on the docked CLD. Figure 4*E* shows that in WT glands, WGA staining intensity on plasma membrane regions directly adjacent to docked CLDs is reduced compared to that on plasma membrane regions distal to docking sites. The WGA staining in the dock is reduced to 40% of that in the membrane where no CLDs are docked. In contrast, WGA staining in regions of the membrane over CLDs in MGKO glands is comparable to that found in regions distal to CLDs. In addition, we found that the WGA and Plin2 fluorescence at docking sites in WT gland closely overlap and are not resolvable with the confocal microscope, indicating a separation of <300 nm. As noted above for Plin2 and Btn, peak Plin2 and WGA fluorescence intensities in MGKO are well resolved, with an average distance between peak Plin2 and the WGA intensities of 600 nm. Taken together, these data argue that CLD in XOR MGKO cells are not docking at the membrane.

## CideA mediates CLD fusion and docking

CideA knockout mice were previously shown to have disrupted MFG secretion (Wang *et al.* 2012) related to XOR depletion in the mammary gland. We wanted to see if CideA might have other roles in milk fat secretion, or if the two proteins might be directly interacting, so we immunostained glands for CideA (Fig. 5). In both WT and XOR MGKO glands, we see an association of CideA with the CLDs in the cytoplasm, and concentrated foci of CideA at the fusion pore of two fusing CLDs (Fig. 5*B*). At focal contact sites between lipid droplets, CideA promotes directional net neutral lipid transfer from the smaller to larger lipid droplets (Wu *et al.* 2014; Barneda *et al.* 2015). However, we also see bright CideA staining in the docking site in WT glands, but not in MGKO glands (Fig. 5*A*, arrowheads). We also measured the size of the CLD at the APM in sections from WT and MGKO glands. We see larger CLDs in MGKO than WT (median 12.6 *vs* 4.5 $\mu$m), 22-fold larger by volume, suggesting that delayed secretion and CideA-mediated fusion may be resulting in larger droplets.

## Very large lipid droplets are secreted into the milk of XOR MGKO glands

Our histological and immunofluorescence data indicate that in the absence of XOR, CLDs are unable to undergo apical membrane docking, which we speculated was required for envelopment and secretion. Thus, we expected that milk produced by MGKO mice would lack or be deficient in lipid. Surprisingly, we found that the volume per cent of fat in milk at L10, from MGKO dams (50±7, $n = 13$) is actually significantly ($P<0.01$) greater than that of WT dams (36±9, $n = 11$) (Fig. 6*A*). We visualized and measured these secreted globules by staining with the neutral lipid stain, BODIPY 493/503. The size of secreted MFGs from CideA null mice was smaller than that observed in milk from WT mice (Wang, 2012). In contrast, the size of MFGs isolated from L10 milk of the XOR MGKO dams was significantly greater than that of WT (Fig. 6*B*, *C*). In total, 80% of the MFGs in WT milk are smaller than 9 $\mu$m in diameter, whereas only 40% fall into this size range in the MGKO milk. When we calculate the fractional volume of lipid in each size range, the difference in secretion mechanism is highlighted. More than 80% of the total secreted lipid is present in globules greater than 12 $\mu$m in diameter in the MGKO milk, while this fraction accounts for less than 20% of the lipid in WT milk (Fig. 6*C*, yellow, orange, red, purple bars). These data suggest that in the absence of XOR, large CLDs in mammary glands of MGKO mice, unable to dock, nevertheless undergo engulfment and secretion by a modified apical membrane inclusion process. This altered secretory mechanism delays lipid release, resulting in larger CLD and larger secreted

globules. Interestingly, doubling the size of the CLD (from 8 to 16 $\mu$m) requires 52% less membrane per unit volume of lipid, for engulfment. Increasing the diameter of the lipid droplet thus changes the ratio of neutral lipid to phospholipid, and changes the proportion of membrane required for secretion. We speculate that the loss of docking also makes the sorting of cellular materials for secretion less efficient.

## XOR loss alters the proteome of MFGs

The modified apocrine secretion mechanism discussed above suggests that the protein composition of MFGs from MGKO mice should differ significantly from that of WT MFGs in both the number and the type of proteins. To test this prediction we used untargeted proteomic analysis of MFGs from WT and MGKO mice. LC-MS/MS analysis of isolated and washed MFGs obtained from lactating dams at L10 identify an average of 18,000 spectra per run for a total of 730 proteins. Protein identifications were accepted if they could be established at greater than 99.0% probability and contained at least two identified unique peptides. Using these criteria, 592 proteins are identified as being present in MFG samples from WT mice and 651 proteins are present in XOR-MGKO samples. In total, 505 proteins found on MFGs from both WT and XOR-MGKO mice are used in a volcano plot analysis (Bessarabova *et al.* 2012) of the fold-change between

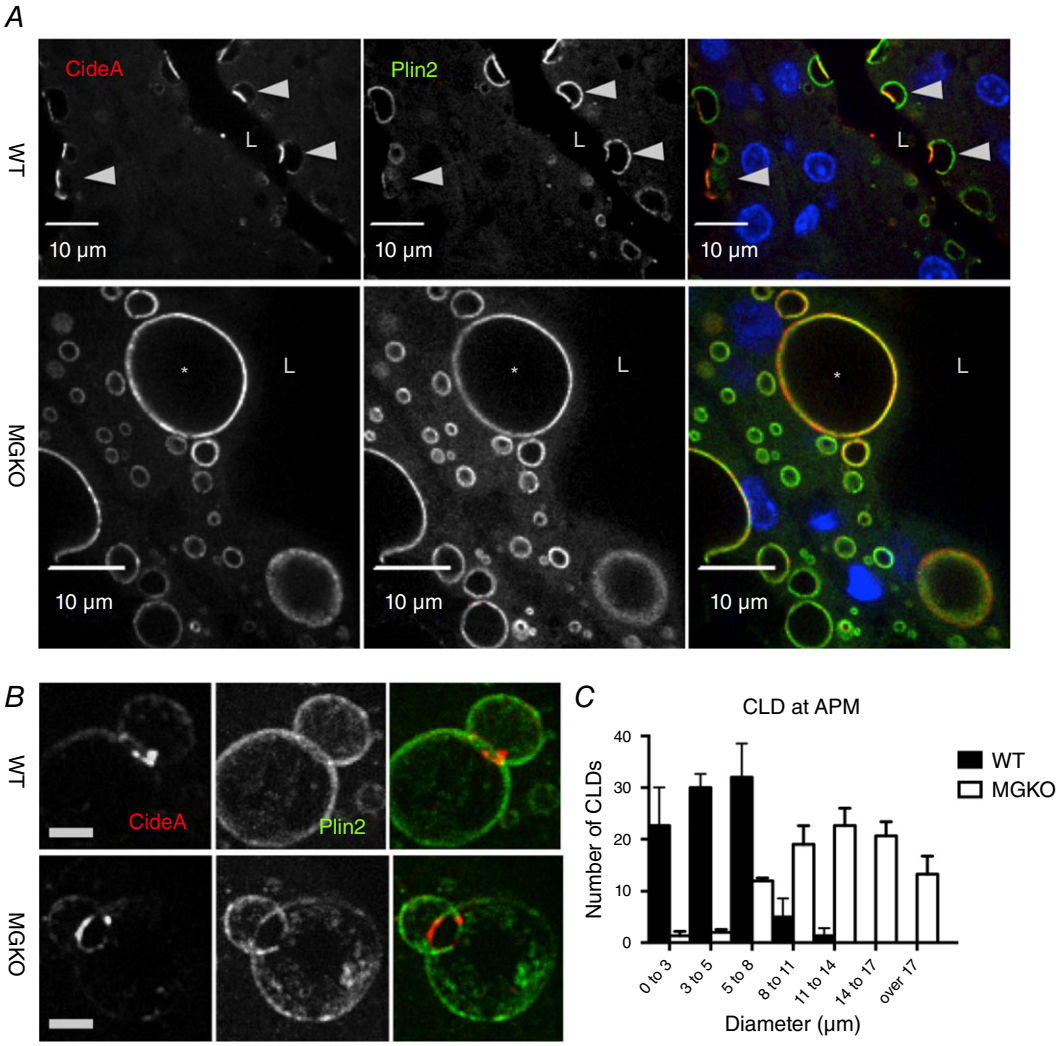


**Figure 5. CideA mediates CLD fusion and docking**
*A*, L10 mammary gland from WT and XOR MGKO dams immunostained for CideA (red, right), Plin2 (green, centre) and DAPI (blue in overlay). Arrowheads delineate docked CLDs with CideA clustered. Asterisk marks a large CLD that is not docked. Bar = 10 $\mu$m. *B*, 3D projection view of fusing CLDs. CideA (right, red), Plin2 (centre, green) and overlay showing CideA concentrated at the fusion pore of two CLDs in WT and MGKO glands. Bar = 2 $\mu$m. *C*, pre-secretion CLD sizes measured in the cytoplasm near the apical plasma membrane (APM) in Plin2-stained WT and XOR MGKO cells (>50 CLDs per mouse, three mice per group).

their spectral counts *versus* significance (Fig. 7). This plot reveals an essential asymmetry, an increase in abundance of proteins associated with the MGKO globules. The most significantly increased proteins were not predicted, but include (1) glutamyl-prolyl-tRNA synthetase (Eprs), which is 26-fold increased and forms a node connecting cytoskeletal and vesicular trafficking networks (see Strings Analysis, Fig. 8). Eprs is a 170 kDa, low abundance protein, part of the gamma interferon (IFN-$\gamma$)-activated inhibitor of translation (GAIT) complex, regulating translation of inflammation genes. Co-factors of Eprs include ribosomal protein L13a, and glyceraldehyde-3-phosphate dehydrogenase (Gapdh), both of which are present in WT and MGKO samples. (2) Lipopolysaccharide

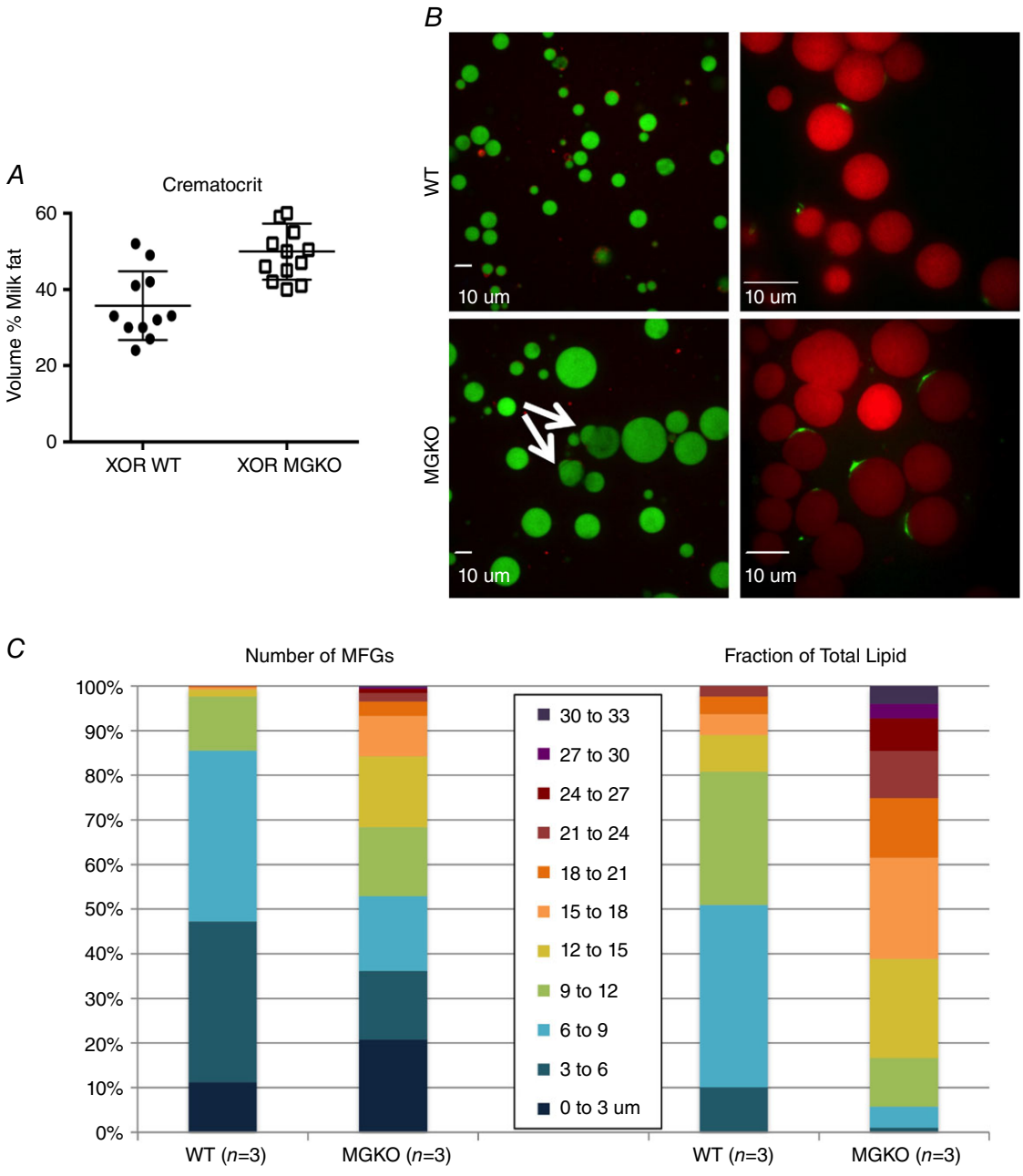


**Figure 6. Very large lipid droplets are secreted into the milk of XOR MGKO glands**
*A*, crematocrit (volume % milk fat) of milk collected from WT (36 ± 9) and MGKO (50 ± 7) dams at lactation day 10 (mean ± SD, $P = 0.0003$). *B*, BODIPY 493/503-stained, post-secretion MFGs (left). Arrows indicate MFGs damaged in the milking process. LipidTox Red and Alexa 488-phalloidin (green) staining of globules from WT and XOR MGKO milk (right). Bar = 10 $\mu$m. *C*, diameter of post-secretion MFGs, stained with BODIPY 493/503 (>800 MFGs per mouse, three mice per group). Size ranges are displayed as a fraction of the total counted and as a fraction of the total lipid volume.

(LPS)-binding protein (Lbp) is 6.2-fold increased. Lbp is part of the innate immune system, thought to bind CD14 in infant gut preventing pathogen binding and internalization. (3) Pnpla2/adipose triglyceride lipase (Atgl) is 4.7-fold increased. Pnpla2/Atgl is a possible regulator of CLD size. It interacts with Abhd5/CGI-58, which is also increased 1.7-fold in MGKO. (4) Tubulin alpha 1b (Tuba1b), which is a node within the cytoskeletal network (Fig. 8), is 11-fold increased. Tubulin alpha 4a and beta 4b were also present in MGKO but were entirely absent from WT MFG samples.

Identified proteins are further categorized according to Gene Ontology cellular component terms (Table 1). We see statistically significant increases in the number of cytoplasmic, cytoskeletal, Golgi apparatus and lipid metabolism proteins that remain associated with the secreted MFGs in the MGKO samples. However, proteins associated with the endoplasmic reticulum, mitochondria, plasma membrane and vesicle-mediated transport are not increased in number, suggesting that the loss of XOR changes the MFG secretory process, allowing inclusion of proteins/organelles that are typically retained within the cell. As suggested by the immunostains above, the XOR MGKO gland may depend on increased Golgi vesicle involvement to mediate MFG secretion (Wooding *et al.* 2015). However, a detailed, high-resolution electron microscopy study of this knockout would be necessary to discern the changes in CLD association with organelles, and ultrastructural differences in the APM association.

To further characterize the proteins and enzymes associated with the MFGs, we use the normalized spectral abundance factor (NSAF) (Paoletti *et al.* 2006) for each protein to estimate how XOR loss changes protein components quantitatively. A partial list of NSAFs showing the proteins with significant differences between WT and MGKO globules, ranked by fold change, is given in Table 2 and the entire dataset is given as supplementary data (Table S1). The most abundant protein in MFGs from both WT and XOR MGKO mice is lactadherin/Mfg-e8, a peripheral membrane protein thought to bind to phosphatidylserine on the external leaflet of the APM, and its levels are unchanged. The levels of XOR in MGKO MFGs are reduced by 97% compared to its levels in WT MFGs. Significantly, the ratio of normalized spectral abundance for XOR and Btn in WT MFGs calculated from our MS/MS data is 2:1, which

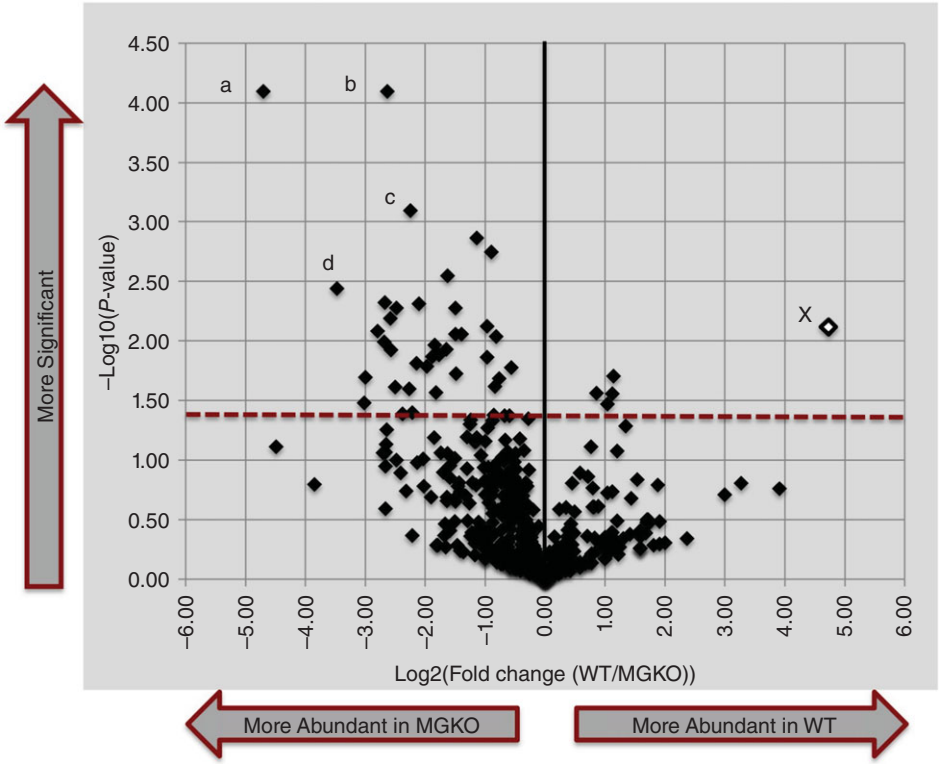


**Figure 7. Volcano plot reveals asymmetry in proteins associated with MFGs from XOR MGKO dam**
Plot of the $\log_2$fold change (WT/MGKO) of the spectral abundance *versus* the $\log_{10}$(*P*-value) for the proteome of the MFGs. The empty point is XDH/XOR (marked with an x). The most significantly changed proteins, all in greater abundance on MGKO MFGs are: a, glutamyl-prolyl-tRNA synthetase (EPRS), 26-fold increased; b, lipopolysaccharide (LPS)-binding protein (LBP), 6.2-fold increased; c, Pnpla2, a.k.a. adipose triglyceride lipase (Atgl), 4.7-fold increased; d, tubulin alpha 1b (Tuba1b), 11-fold increased. [Colour figure can be viewed at wileyonlinelibrary.com]

agrees with the published ratio obtained by biochemical measurements (McManaman *et al.* 2002) and provides evidence of the validity of comparisons made using NSAF. Proteins with reduced levels in the MGKO globules are rare and include butyrophilin (Btn, 63% reduced), fibrinogen-$\beta$ and -$\gamma$ chains (Fgb and Fgg, reduced by 57 and 58%, respectively), and apolipoprotein C-III (Apoc3, reduced by 50%). The proportional reduction in these four proteins (Btn/Fgg/Fgb/Apoc3) suggests that they may be present in a complex on the APM (ratio 1:2:2:1) prior to

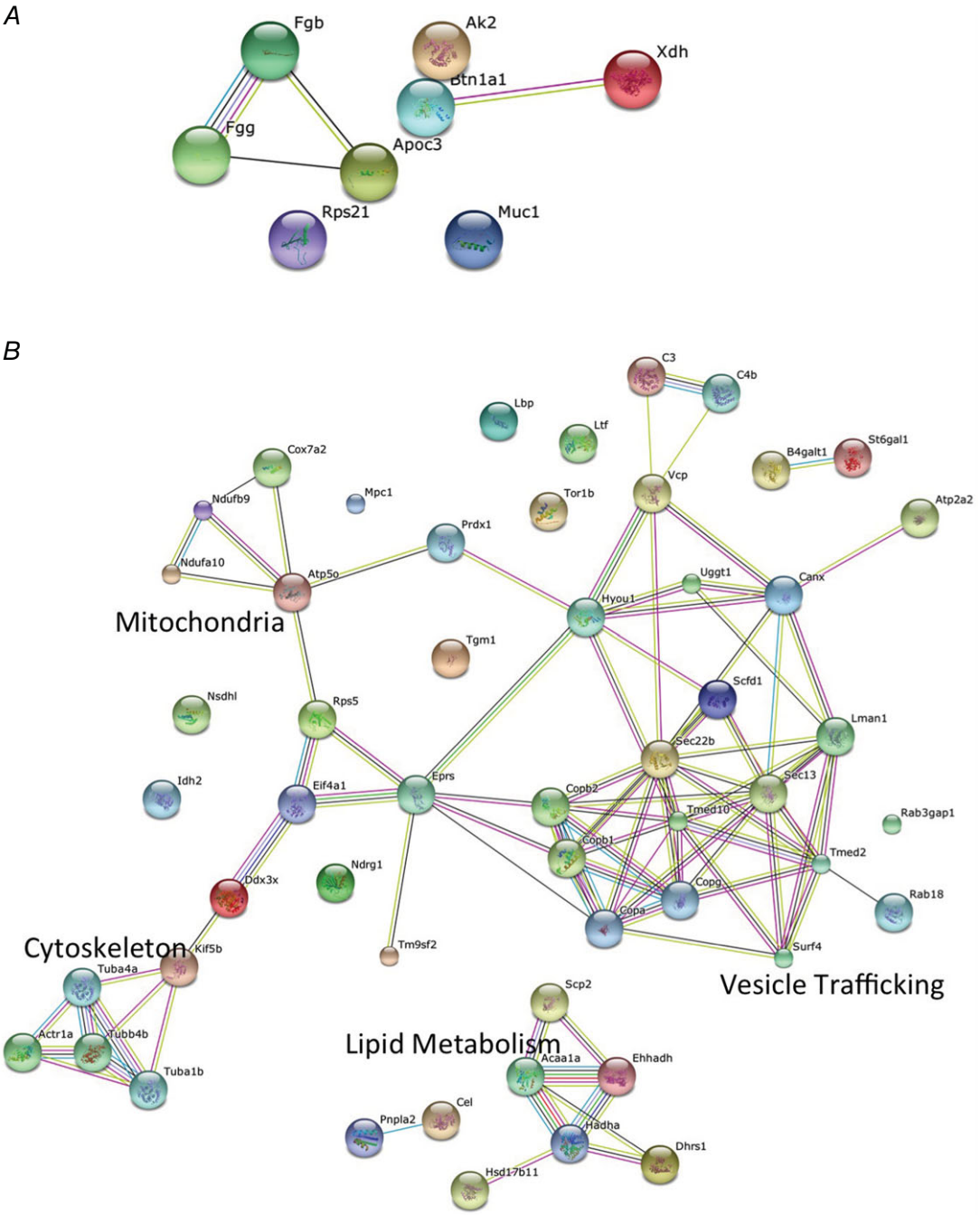


**Figure 8. String networks of proteins significantly changed on MFGs from WT and XOR MGKO dams reveal interacting proteins**
*A*, only eight proteins are significantly lost from the MFGs when XOR (XDH) is genetically deleted (see Table 2). XOR is known to interact with Btn. Fgg, Fgb and Apoc3 also interact. *B*, 52 proteins are significantly increased on the MFGs when XOR is deleted. Labelled are nodes related to vesicle trafficking, lipid metabolism and cytoskeleton. [Colour figure can be viewed at wileyonlinelibrary.com]

**Table 1. Total number of cytoplasmic, cytoskeletal, Golgi apparatus and lipid metabolism proteins are increased on MFGs from XOR MGKO dams, indicating changes in efficiency of secretion; Gene Ontology (GO) analysis of subcellular organelles**

| GO term | No. of proteins | WT (mean ± SEM) | MGKO (mean ± SEM) | *t*-test |
|---|---|---|---|---|
| **Cytoplasmic** | 607 | 340 ± 27 | 410 ± 9 | **0.048** |
| **Cytoskeleton** | 84 | 37 ± 1 | 53 ± 3 | **0.005** |
| Endoplasmic reticulum | 95 | 76 ± 4 | 70 ± 4 | 0.308 |
| Ribosomal | 73 | 55 ± 4 | 58 ± 4 | 0.666 |
| Mitochondria | 242 | 147 ± 15 | 163 ± 5 | 0.372 |
| **Lipid metabolism** | 84 | 48 ± 3 | 61 ± 3 | **0.021** |
| Plasma membrane | 112 | 82 ± 5 | 87 ± 5 | 0.524 |
| Vesicle-mediated transport | 63 | 33 ± 3 | 42 ± 3 | 0.075 |
| **Golgi apparatus** | 67 | 32 ± 4 | 46 ± 5 | **0.017** |

Shown are the total number of proteins in each GO category identified and the mean numbers of proteins from $n = 4$ dams in each group, ± SEM and *P*-value using Student's *t*-test. *P*-value $< 0.05$ indicated in bold.

being recruited into a complex with XOR at the site of CLD binding. Adenylate kinase 2 (Ak2) is similarly reduced and while it is thought of as an enzyme localized to the inner mitochondrial membrane, it catalyses the reversible transfer of the terminal phosphate groups between ATP and AMP, and thus may be involved in regulation of purine metabolism, or depletion of ATP in the microvilli. It is present in a (1:4) ratio with Btn in our samples, independent of genotype. Only two proteins are lost entirely from XOR-MGKO MFGs including Muc1, a major mucin present on the apical surface of milk-secreting cells, and ribosomal protein S21 (Rps21), a component of the 40S subunit of the ribosome. We assess possible functional interactions among these proteins using string analysis (http://string-db.org/) (Fig. 8*A*). In addition to the known interaction between XOR and Btn, interactions among the fibrinogens and ApoC3 are also predicted.

Ten proteins are found exclusively in the MFGs from MGKO dams. These include two tubulins (Tuba4a, Tubb4b), a Rab-GTPase activating protein (Rab3gap1), a secretory protein (Scfd1), a non-specific lipid transfer protein (Scp2), a calcium ATPase (Atp2a2), a sialyltransferase (Stgal1), a transmembrane superfamily member (Tm9sf2) Torsin-1B (Tor1b) and alpha-centractin (Actr1a). Abundances of 41 proteins are increased significantly by XOR loss. String analysis shows that they are enriched in functional networks corresponding to: vesicle trafficking, which includes a node for coatmers (Copa, Copb1, Copb2, Copg); lipid metabolism, which includes nodes for lipid oxidation and lipase activities; the cytoskeleton, which includes a tubulin node; and the mitochondria, which includes a node linking oxidase, dehydrogenase and ATPase activities (Fig. 8*B*). Of interest, only two proteins among the 50 most abundant are increased in the MGKO globules, including Rab18, a small GTP-binding protein known to be important for lipid droplet and vesicle trafficking, and Dhrs1, a member of the short-chain dehydrogenases/reductases family (SDR) of enzymes, most of which are known to be NAD- or NADP-dependent oxidoreductases. Both of these proteins were shown to be associated with the CLD of 3T3-L1 adipocytes under conditions that stimulate lipolysis (Brasaemle *et al.* 2004).

Because the lipid droplets in XOR MGKO glands are larger, we further compared proteins associated with the Gene Ontology term 'Lipid Metabolism'. Supplementary Table S1 shows the NSAF and fold change for proteins that are present in all four MGKO samples. Notably, three lipases, known to facilitate lipid breakdown, Pnpla2, Cel and Lpl, are increased on the MGKO globules, despite their significantly larger size. It is unclear whether the alveolar cell is actively trying to reduce these oversized CLD prior to secretion, or whether these lipases are not enzymatically active. Several other proteins change proportionally in the MGKO samples, possibly suggesting a direct molecular interaction. Included are Nsdhl and Ehhadh (1:1), Pnpla2 and Cel and Hsd17b7 (2:2:1), Tecr and Hadha and Dbt (1:2:1), Abhd5 and Acaa2 (2:1), CideA and Acsl1 (1:1), and Atp5a1 and Atp5b and Fasn (1:2:1). Of these, only Atp5a1 and Atp5b have been previously shown to be functionally interacting proteins. Despite the larger CLDs, lipid synthesis enzymes do not seem to be preferentially enriched on the secreted globules. Thus, we speculate that the increased size of the droplets is due to CideA-mediated fusion of smaller CLDs during delayed secretion.

Inclusions of cytoplasmic components within the membrane of the final, secreted MFGs are called crescents, and were described in early electron micrographs of milk and lactating glands. (Wooding *et al.* 1970; reviewed by Huston & Patton, 1990). The proteomics results described above suggest that there may be a modest increase in these crescents associated with the globules from XOR MGKO milk. Electron micrographs (Fig. 2*D* and *H*) show crescents attached to secreted globules in the lumens of both the WT and the XOR MGKO glands. Additionally, we stained milk droplets with Acridine Orange (data not

**Table 2. Normalized spectral abundance factor (NSAF), a measure of protein abundance, for the MFG proteome of WT and MGKO dams**

| NSAF | | | | | MFG proteome | | | | XOR f/f x BLG-Cre |
|---|---|---|---|---|---|---|---|---|---|
| WT ($n = 4$) | SD | MGKO ($n = 4$) | SD | Gene | Proteins significantly changed by loss of XOR | Accession | *t*-test | Fold change | Function |
| 0.19 | 0.10 | 0.00 | 0.00 | Muc1 | Mucin-1 | Q02496 | **0.0094** | 0.00 | Epithelial barrier |
| 0.34 | 0.24 | 0.00 | 0.00 | Rps21 | 40S ribosomal protein S21 | Q9CQR2 | **0.0307** | 0.00 | Ribosome |
| 10.7 | 4.1 | 0.37 | 0.30 | Xdh | Xanthine dehydrogenase/oxidase | Q00519 | **0.0025** | 0.03 | Purine degradation, oxidoreductase, milk lipid secretion |
| 4.98 | 2.02 | 1.84 | 0.60 | Btn1a1 | Butyrophilin subfamily 1 member A1 | Q62556 | **0.0245** | 0.37 | Milk lipid secretion |
| 10.2 | 3.5 | 4.33 | 1.39 | Fgg | Fibrinogen gamma chain | Q8VCM7 | **0.0215** | 0.42 | Clotting |
| 10.7 | 3.9 | 4.62 | 1.38 | Fgb | Fibrinogen beta chain | Q8K0E8 | **0.0277** | 0.43 | Clotting |
| 1.33 | 0.46 | 0.60 | 0.09 | Ak2 | Adenylate kinase 2, mitochondrial | Q9WTP6 | **0.0210** | 0.45 | Purine salvage |
| 4.83 | 1.58 | 2.46 | 0.56 | Apoc3 | Apolipoprotein C-III | P33622 | **0.0324** | 0.51 | Triglyceride homeostasis |
| 0.82 | 0.19 | 1.13 | 0.09 | Rps5 | 40S ribosomal protein S5 | P97461 | **0.0235** | **1.4** | Ribosome |
| 1.09 | 0.30 | 1.56 | 0.18 | Atp5o | ATP synthase subunit O, mitochondrial | Q9DB20 | **0.0349** | **1.4** | Mitochondrial ATP synthesis |
| 0.45 | 0.17 | 0.72 | 0.07 | Ndufa10 | NADH dehydrogenase [ubiquinone] 1 alpha subcomplex subunit 10, mitochondrial | Q99LC3 | **0.0343** | **1.6** | Mitochondrial e- transport |
| 0.20 | 0.08 | 0.33 | 0.03 | Ddx3x | ATP-dependent RNA helicase DDX3X | Q62167 | **0.0192** | **1.6** | Ribosome |
| 1.84 | 0.56 | 3.07 | 0.59 | Dhrs1 | Dehydrogenase/reductase SDR family member 1 | Q99L04 | **0.0189** | **1.7** | Oxidoreductase |
| 0.44 | 0.18 | 0.75 | 0.18 | Hyou1 | Hypoxia up-regulated protein 1 | Q9JKR6 | **0.0465** | **1.7** | Chaperone |
| 0.51 | 0.27 | 0.88 | 0.10 | Hadha | Trifunctional enzyme subunit alpha, mitochondrial | Q8BMS1 | **0.0398** | **1.7** | Mitochondrial b-oxidation |
| 0.97 | 0.28 | 1.67 | 0.09 | Tmed10 | Transmembrane emp24 domain-containing protein 10 | Q9D1D4 | **0.0031** | **1.7** | ER >Golgi transport |
| 0.72 | 0.18 | 1.32 | 0.30 | Surf4 | Surfeit locus protein 4 | Q64310 | **0.0114** | **1.8** | ER >Golgi transport |
| 2.40 | 0.69 | 4.41 | 0.65 | Rab18 | Ras-related protein Rab-18 | P35293 | **0.0061** | **1.8** | Vesicle transport |
| 0.38 | 0.14 | 0.78 | 0.04 | Vcp | Transitional endoplasmic reticulum ATPase | Q01853 | **0.0023** | **2.1** | ER ATPase |
| 0.11 | 0.09 | 0.25 | 0.06 | Canx | Calnexin | P35564 | **0.0408** | **2.4** | Protein folding |
| 0.25 | 0.17 | 0.62 | 0.10 | Lman1 | Protein ERGIC-53 | Q9D0F3 | **0.0079** | **2.5** | ER >Golgi cargo receptor |

(*Continued*)

**Table 2. Continued**

| NSAF | | | | | MFG proteome | | | | XOR f/f x BLG-Cre |
|---|---|---|---|---|---|---|---|---|---|
| WT ($n = 4$) | SD | MGKO ($n = 4$) | SD | Gene | Proteins significantly changed by loss of XOR | Accession | *t*-test | Fold change | Function |
| 0.28 | 0.18 | 0.73 | 0.14 | Tmed2 | Transmembrane emp24 domain-containing protein 2 | Q9R0Q3 | **0.0082** | **2.6** | ER >Golgi transport |
| 0.14 | 0.07 | 0.37 | 0.09 | Tgm1 | Protein-glutamine gamma-glutamyltransferase K | Q9JLF6 | **0.0160** | **2.6** | Protein cross-linking |
| 0.08 | 0.08 | 0.22 | 0.03 | Idh2 | Isocitrate dehydrogenase [NADP], mitochondrial | P54071 | **0.0220** | **2.8** | Mitochondrial b-oxidation |
| 0.28 | 0.10 | 0.81 | 0.19 | B4galt1 | Beta-1,4-galactosyltransferase 1 | P15535 | **0.0030** | **2.9** | Golgi-anchored, lactose synthesis |
| 0.04 | 0.03 | 0.10 | 0.03 | Uggt1 | UDP-glucose:glycoprotein glucosyltransferase 1 | Q6P5E4 | **0.0134** | **2.9** | Unfolded protein response |
| 0.09 | 0.09 | 0.32 | 0.09 | Copa | Coatomer subunit alpha | Q8CIE6 | **0.0119** | **3.5** | Non-clathrin-coated vesicle transport |
| 0.10 | 0.13 | 0.36 | 0.06 | Ndrg1 | Protein NDRG1 | Q62433 | **0.0100** | **3.6** | Lipid trafficking, microtubule dynamics |
| 0.09 | 0.11 | 0.32 | 0.10 | Copg1 | Coatomer subunit gamma-1 | Q9QZE5 | **0.0228** | **3.6** | Non-clathrin-coated vesicle transport |
| 0.11 | 0.15 | 0.40 | 0.08 | Sec 22b | Vesicle-trafficking protein SEC22b | O08547 | **0.0178** | **3.8** | ER >Golgi transport |
| 0.08 | 0.07 | 0.33 | 0.09 | Copb2 | Coatomer subunit beta' | O55029 | **0.0074** | **4.0** | Non-clathrin-coated vesicle transport |
| 0.07 | 0.09 | 0.29 | 0.09 | Copb1 | Coatomer subunit beta | Q9JIF7 | **0.0199** | **4.0** | Non-clathrin-coated vesicle transport |
| 0.21 | 0.11 | 0.85 | 0.35 | Cel | Bile salt-activated lipase | Q64285 | **0.0144** | **4.1** | Triglyceride homeostasis |
| 0.06 | 0.08 | 0.27 | 0.12 | Ltf | Lactotransferrin | P08071 | **0.0350** | **4.1** | Host defence |
| 0.18 | 0.12 | 0.80 | 0.15 | Pnpla2 | Patatin-like phospholipase domain-containing protein 2 | Q8BJ56 | **0.0008** | **4.4** | Triglyceride homeostasis |
| 0.08 | 0.15 | 0.34 | 0.13 | Ndufb9 | NADH dehydrogenase [ubiquinone] 1 beta subcomplex subunit 9 | Q9CQJ8 | **0.0398** | **4.5** | Mitochondrial e- transport |
| 0.01 | 0.01 | 0.06 | 0.02 | Kif5b | Kinesin-1 heavy chain | Q61768 | **0.0058** | **5.3** | Motor protein |
| 0.06 | 0.09 | 0.33 | 0.15 | Ehhadh | Peroxisomal bifunctional enzyme | Q9DBM2 | **0.0213** | **5.3** | Peroxisome b-oxidation |
| 0.07 | 0.05 | 0.40 | 0.13 | Eif4a1 | Eukaryotic initiation factor 4A-I | P60843 | **0.0095** | **5.5** | Ribosome |

(*Continued*)

**Table 2. Continued**

| NSAF | | | | | MFG proteome | | | | XOR f/f x BLG-Cre |
|---|---|---|---|---|---|---|---|---|---|
| WT ($n = 4$) | SD | MGKO ($n = 4$) | SD | Gene | Proteins significantly changed by loss of XOR | Accession | *t*-test | Fold change | Function |
| 0.06 | 0.12 | 0.34 | 0.16 | Nsdhl | Sterol-4-alpha-carboxylate 3-dehydrogenase, decarboxylating | Q9R1J0 | **0.0299** | **5.6** | ER cholesterol synthesis |
| 0.04 | 0.04 | 0.21 | 0.08 | C3 | Complement C3 | P01027 | **0.0090** | **5.7** | Clotting + acute phase |
| 0.15 | 0.11 | 0.88 | 0.09 | Lbp | Lipopolysaccharide-binding protein | Q61805 | **0.0000** | **6.1** | Acute phase |
| 0.05 | 0.10 | 0.31 | 0.07 | Acaa1a | 3-Ketoacyl-CoA thiolase A, peroxisomal | Q921H8 | **0.0046** | **6.2** | Peroxisome b-oxidation |
| 0.19 | 0.39 | 1.34 | 0.42 | Cox7a2 | Cytochrome c oxidase subunit 7A2, mitochondrial | P48771 | **0.0071** | **6.9** | Mitochondrial e- transport |
| 0.02 | 0.04 | 0.14 | 0.04 | C4b | Complement C4-B | P01029 | **0.0060** | **7.5** | Clotting + acute phase |
| 0.04 | 0.08 | 0.36 | 0.17 | Mpc1 | Mitochondrial pyruvate carrier 1 | P63030 | **0.0136** | **8.5** | Mitochondrial pyruvate import |
| 0.08 | 0.15 | 0.65 | 0.36 | Hsd17b11 | Estradiol 17-beta-dehydrogenase 11 | Q9EQ06 | **0.0240** | **8.6** | Dehydrogenase/reductase |
| 0.04 | 0.03 | 0.49 | 0.17 | Tuba1b | Tubulin alpha-1B chain | P05213 | **0.0063** | **11** | Cytoskeleton |
| 0.00 | 0.01 | 0.08 | 0.01 | Eprs | Bifunctional glutamate/proline–tRNA ligase | Q8CGC7 | **0.0003** | **28** | Gamma interferon-activated inhibitor of translation |
| 0.00 | 0.00 | 0.26 | 0.05 | Tuba4a | Tubulin alpha-4A chain | P68368 | **0.0001** | **inf** | Cytoskeleton |
| 0.00 | 0.00 | 0.31 | 0.08 | Tubb4b | Tubulin beta-4B chain | P68372 | **0.0003** | **inf** | Cytoskeleton |
| 0.00 | 0.00 | 0.14 | 0.05 | Scp2 | Non-specific lipid-transfer protein | P32020 | **0.0006** | **inf** | Peroxisome b-oxidation *or* intracellular lipid transport |
| 0.00 | 0.00 | 0.08 | 0.03 | Scfd1 | Sec 1 family domain-containing protein 1 | Q8BRF7 | **0.0016** | **inf** | ER > Golgi transport |
| 0.00 | 0.00 | 0.04 | 0.02 | Rab3gap1 | Rab3 GTPase-activating protein catalytic subunit | Q80UJ7 | **0.0024** | **inf** | Vesicle transport |
| 0.00 | 0.00 | 0.08 | 0.05 | Atp2a2 | Sarcoplasmic/endoplasmic reticulum calcium ATPase 2 | O55143 | **0.0261** | **inf** | ER $Ca^{2+}$ export |
| 0.00 | 0.00 | 0.12 | 0.09 | St6gal1 | Beta-galactoside alpha-2,6-sialyltransferase 1 | Q64685 | **0.0279** | **inf** | Golgi glycosylation |
| 0.00 | 0.00 | 0.11 | 0.08 | Tm9sf2 | Transmembrane 9 superfamily member 2 | P58021 | **0.0358** | **inf** | Endosome thiol exchange |
| 0.00 | 0.00 | 0.10 | 0.08 | Tor1b | Torsin-1B | Q9ER41 | **0.0447** | **inf** | ER integrity, poss chaperone |
| 0.00 | 0.00 | 0.13 | 0.10 | Actr1a | Alpha-centractin | P61164 | **0.0471** | **inf** | ER >Golgi transport |

Shown are means ± SD for $n = 4$ mice per group, of only the proteins whose abundance is significantly changed as assessed by Student's *t*-test. The gene name, common protein name and accession are listed for each protein, as well as the fold change (MGKO/WT) and the putative function of each protein. The NSAF of the entire proteome from each group is given as supporting data. Fold-changes >1 (higher in MGKO) are shown in bold.

shown), and with a combination of LipidTox Red to stain the neutral lipid, and phalloidin to visualize the filamentous actin, in order to visualize these crescents (Fig. 6*B*). In both the WT and the XOR MGKO, obvious crescents were present in 25% of the globules. There was no change in the fraction of globules with crescents, although there may have been a small (not significant) change in the size of the attached cytoplasmic crescent in the XOR MGKO MFGs. This result is consistent with the results of the proteomics data above. The abundance of actin is increased only 1.5-fold, and similarly the keratins, a family of cytoplasmic intermediate filament proteins, have an average increase of 1.8- to 2.0-fold in the XOR MGKO globules. These changes did not reach significance, and further support the notion that even without docking, apocrine secretion of CLDs can occur. The process is slightly less efficient, as some cellular components that should be retained are not, possibly requiring new synthesis of these proteins. The growth rates of the pups from XOR MGKO dams are only 20% less than those of the WT dams, suggesting that the back-up mechanism of milk fat secretion is adequate.

## Discussion

Previous work has shown loss of XOR results in total lactation failure (Vorbach *et al.* 2002; Wang *et al.* 2012). However, those studies were performed in knockout models which may have had deleterious effects on the physiology of the dam, due to loss of XOR in the liver or adipose tissue. In our conditional knockout models, removing XOR protein in the mammary epithelial cells alone results in only a modest lactation defect. We did observe that XOR mediates close association between the CLD and elements of the APM, a process we call 'docking'. XOR is also required for Btn membrane clustering during milk lipid secretion, presumably drawing Btn into the membrane domain where CLDs are docked. Additionally, XOR mediates apical membrane reorganization during milk lipid secretion, as docking of CLDs to the membrane disassembles the microvilli and remodels the glycocalyx. Finally, loss of XOR seems to delay MFG secretion, which allows continued growth and/or fusion of CLDs. Significantly, loss of XOR does not prevent membrane envelopment of CLDs or their secretion. However, the envelopment process appears to be substantially altered in the absence of XOR, as we see pronounced invagination of the apical membrane in MGKO glands that may be mediated by sequential vesicular trafficking, creating a lumen beneath the CLDs. There is an overall increase in the number of cytoplasmic, cytoskeletal, Golgi apparatus and lipid metabolism proteins associated with the secreted MFGs from XOR MGKO dams, suggesting that cellular components that are usually retained in the cell are present within the budded MFG membrane. Based on these data, we propose that XOR interactions with Btn mediate membrane docking of CLDs, which enhances the efficiency, but is not required for apocrine secretion of milk lipids.

The model of milk fat secretion originally described by Mather & Keenan (1998), utilizing the three proteins ADPH/Plin2 on the CLD, XOR recruited from the cytoplasm and Btn within the APM is supported by the data presented here. Loss of XOR resulted in inefficient MFG secretion, as evidenced by the continued growth and fusion of the CLD before release into the milk. Additionally, loss of XOR results in a decrease in the Btn associated with the secreted MFG, suggesting that XOR recruits or clusters the Btn present in the plasma membrane in a discrete docking step. Fluorescence recovery after photobleaching (FRAP) of GFP-Btn1a1 in MFG membranes (Jeong *et al.* 2013) described these two populations of Btn, one with rapid recovery after photobleaching, presumably mobile in the membrane, and another that was less mobile, probably bound to XOR and the CLD. Thus, XOR appears to be necessary for this docking step and the idea given by Robenek *et al.* (2006), in which Btn-alone tethers the CLD to the membrane, seems to be contradicted by our data, and similarly, with the model proposed by Chong *et al.* (2011) that Plin2 alone can mediate binding of the CLD to the plasma membrane. Plin2 levels were unchanged on the globules yet CLDs were never observed in close apposition to the apical plasma membrane in our XOR MGKO glands. However, Plin2 probably does play a role in the association of the CLD with other, internal membranes, such as endoplasmic reticulum, peroxisomal or mitochondrial membranes (reviewed by Brasaemle and Wolins, 2012), and with cytoskeletal elements controlling CLD trafficking (Orlicky *et al.* 2013). Finally, what mediates XOR binding to the CLDs docked at the apical membrane remains unknown. As CideA appears to be present in the dock, interactions between XOR and CideA should perhaps be explored further.

Thus far unexplained is the decreased growth rate of the litters nursed on XOR MGKO dams. We analyse the histology of the mammary glands of pregnancy in the BLG–Cre cross and see no difference in growth of the epithelium, alveolar development or differentiation as evidenced by CLD synthesis, casein expression and luminal expansion. However, XOR may have additional roles in neonatal development, such as modulation of the microbiome, which could alter growth of the litter. XOR activity in human milk has been shown to react with xanthine in the saliva in the baby, producing bactericidal ROS (Al-Shehri *et al.* 2015). And Silanikove *et al.* (2005) have shown XOR-derived ROS control bacterial growth in cow's milk. The increase in MFG-associated LPS-binding protein (Lbp) in our proteome thus could indicate that in the absence of XOR, microbial growth in the gland is

uncontrolled, as Lbp level in cow's milk has been shown to be increased with mastitis (Zeng *et al.* 2009). It is likely that these changes in the milk affect the immature gut of the neonate, modulating intestinal development, nutrient absorption and growth. Studies are ongoing along this line of research.

Others have noted that as MFG size increases, the percentage fat in the milk also increases, (reviewed by Jeong *et al.* 2013) and we see both of these changes in our XOR MGKO milk. As lipid droplet size increases, the surface to volume ratio actually decreases, and therefore larger CLDs require less membrane for engulfment and secretion. The secretion of milk products by vesicle exocytosis may be intricately tied to the secretion of milk lipid. Indeed, Farkas (2015) in his review of the mechanisms of apocrine secretion, mentions that merocrine secretion, for example the exocytosis of caseins and lactose, may be linked to the apocrine secretory process. In the mouse mammary gland, membrane derived from exocytotic vesicles is thought to contribute to the final membrane surrounding the secreted MFGs (Kralj *et al.* 1992). If exocytosis and MFG secretion are mechanistically linked by the regulation of APM surface area, then inefficient secretion of milk fat, as seen in the XOR MGKO gland, may result in less total milk secretion. Further analysis, perhaps with tracer studies, is necessary to determine if milk protein secretion or lactose synthesis may be altered in cells lacking XOR. Analysis of the alveolar cell metabolome during lactation, the milk metabolome, as well as expression analysis of milk synthetic enzymes would answer these questions.

The process of milk fat secretion is a fascinating example of apocrine secretion by a mucosal epithelium. The molecular players mediating apocrine secretion are just beginning to be explored. Farkas (2015) recently reviewed this process, comparing the proteomes of several human fluids secreted by this mechanism and compiling a list of 122 common proteins that may be crucial. Of interest, XOR was not found in all of the fluids studied, but was discussed as being present in milk, tears and bile secretions. It is interesting to note that all of these secretions contain a lipid component. Thus, XOR may mediate apocrine secretion of lipids in other tissues as well.

Apocrine secretion is a poorly studied cellular process as it does not occur outside of a tissue context. Others have reported lipid release from primary mammary cell culture (Cohen *et al.* 2015), but none has visualized the process, nor presented analysis of the structure of the resulting globules. Farkas *et al.* (2014) suggest that *Drosophila* salivary glands could be a useful model system to study apocrine secretion, especially for understanding the sorting of cellular components for secretion and retention within the cell. However, the eventual cell death of this epithelium after major apocrine secretory processes makes it substantively different from the lactating mammary cell, which must continue apocrine secretion for days, weeks or even months. Advancement in 3D-culture of mammary cells may yet enable live imaging of milk secretion (Campbell *et al.* 2011; Mroue and Bissell, 2013), but the external location of the mammary gland, the short generation time of the mouse and the power of genetic modification, along with advances in imaging of cellular processes in live animals, suggest that apocrine secretion of MFGs might now be studied in the lactating animal.

## References


Affolter M, Grass L, Vanrobaeys F, Casado B & Kussmann M (2010). Qualitative and quantitative profiling of the bovine milk fat globule membrane proteome. *J Proteomics* **73**, 1079–1088.

Al-Shehri SS, Knox CL, Liley HG, Cowley DM, Wright JR & Henman MG, Hewavitharana AK, Charles BG, Shaw PN, Sweeney EL & Duley JA (2015). Breastmilk-saliva interactions boost innate immunity by regulating the oral microbiome in early infancy. *PLoS One* **10**, e0135047.

Barneda D, Planas-Iglesias J, Gaspar ML, Mohammadyani D, Prasannan S, Dormann D, Han GS, Jesch SA, Carman GM, Kagan V, Parker MG, Ktistakis NT, Klein-Seetharaman J, Dixon AM, Henry SA & Christian M (2015). The brown adipocyte protein CIDEA promotes lipid droplet fusion via a phosphatidic acid-binding amphipathic helix. *Elife* **4**, e07485.

Bessarabova M, Ishkin A, JeBailey L, Nikolskaya T & Nikolsky Y (2012). Knowledge-based analysis of proteomics data. *BMC Bioinformatics* **13**, S13.

Brasaemle DL, Dolios G, Shapiro L & Wang R (2004). Proteomic analysis of proteins associated with lipid droplets of basal and lipolytically stimulated 3T3-L1 adipocytes. *J Biol Chem* **279**, 46835–46842.

Brasaemle DL & Wolins NE (2012). Packaging of fat: an evolving model of lipid droplet assembly and expansion. *J Biol Chem* **287**, 2273–2279.

Campbell JJ, Davidenko N, Caffarel MM, Cameron RE & Watson CJ (2011). A multifunctional 3D co-culture system for studies of mammary tissue morphogenesis and stem cell biology. *PLoS One* **6**, e25661.

Chong BM, Reigan P, Mayle-Combs KD, Orlicky DJ & McManaman JL (2011). Determinants of adipophilin function in milk lipid formation and secretion. *Trends Endocrinol Metab* **22**, 211–217.

Cohen B-C, Shamay A & Argov-Argaman N (2015). Regulation of lipid droplet size in mammary epithelial cells by remodeling of membrane lipid composition—a potential mechanism. *PLoS One* **10**, e0121645.

DePeters EJ & Hovey RC (2009). Methods for collecting milk from mice. *J Mammary Gland Biol Neoplasia* **14**, 397–400.

Dickow JA, Larsen LB, Hammershøj M & Wiking L (2011). Cooling causes changes in the distribution of lipoprotein lipase and milk fat globule membrane proteins between the skim milk and cream phase. *J Dairy Sci* **94**, 646–656.

Farkaš R, Ďatková Z, Mentelová L, Löw P, Beňová-Liszeková D, Beňo M, Sass M, Řehulka P, Řehulková H, Raška O, Kováčik L, Šmigová J, Raška I & Mechler BM (2014). Apocrine secretion in Drosophila salivary glands: subcellular origin, dynamics & identification of secretory proteins. *PLoS One* **9**, e94383.

Farkaš R (2015). Apocrine secretion: New insights into an old phenomenon. *Biochim Biophys Acta* **1850**, 1740–1750.

Figard L & Sokac AM (2014). A membrane reservoir at the cell surface: unfolding the plasma membrane to fuel cell shape change. *Bioarchitecture* **4**, 39–46.

Fini MA, Monks J, Li M, Frid M, Pugliese SC, Bratton D, Janssen W, Scarpulla R, Karin M, Stenmark KR & Wright RM (2014). Macrophage xanthine oxidoreductase mediates LPS induced lung inflammatory injury in mice through activation of the Nlrp3 inflammasome and mitochondrial OXPHOS. ATS International Conference. First published online 1 May 2014 as http://www.atsjournals.org/doi/abs/10.1164/ajrccm-conference.2014.189.1_MeetingAbstracts.A2106

Fini MA, Monks J, Li M, Frid MG, Fernandez R, Pugliese SC, Bratton D, Janssen W, Scarpulla R, Karin M, Stenmark KR & Wright RM (2016). Macrophage xanthine oxidoreductase links LPS induced lung inflammatory injury to NLRP3 inflammasome expression and mitochondrial respiration. *Cell Rep* In press.

Harrison R (2006). Review. Milk xanthine oxidase: properties and physiological roles. *Int Dairy J* **16**, 546–554.

Heid, HW & Keenan, TW (2005). Intracellular origin and secretion of milk fat globules. *Eur J Cell Biol* **84**, 245–258.

Huston GE & Patton S (1990). Factors related to the formation of cytoplasmic crescents on milk fat globules. *J Dairy Sci* **73**, 2061–2066.

Ishii T, Aoki N, Noda A, Adachi T, Nakamura R & Matsuda T (1995). Carboxy-terminal cytoplasmic domain of mouse butyrophilin specifically associates with a 150 kDa protein of mammary epithelial cells and milk fat globule membrane. *Biochim Biophys Acta* **1245**, 285–292.

Jeong J, Rao AU, Xu J, Ogg SL, Hathout Y, Fenselau C & Mather IH (2009). The PRY/SPRY/B30.2 domain of butyrophilin 1A1 (BTN1A1) binds to xanthine oxidoreductase: implications for the function of BTN1A1 in the mammary gland and other tissues. *J Biol Chem* **284**, 22444–22456.

Jeong J, Lisinski I, Kadegowda AK, Shin H, Wooding FB, Daniels BR, Schaack J & Mather IH (2013). A test of current models for the mechanism of milk-lipid droplet secretion. *Traffic* **14**, 974–986.

Kralj M, Pipan N, Metka K & Nada P (1992). The role of exocytosis in the apocrine secretion of milk lipid globules in mouse mammary gland during lactogenesis. *Biol Cell* **75**, 211–216.

Liao Y, Alvarado R, Phinney B & Lönnerdal B (2011). Proteomic characterization of human milk fat globule membrane proteins during a 12 month lactation period. *J Proteome Res* **10**, 3530–3541.

Lucas A, Gibbs JA, Lyster RL & Baum JD (1978). Creamatocrit: simple clinical technique for estimating fat concentration and energy value of human milk. *Br Med J* **1**, 1018–1020.

Mather IH & Keenan TW (1998). Origin and secretion of milk lipids. *J Mammary Gland Biol Neoplasia* **3**, 259–73.

McManaman JL, Palmer CA, Wright RM & Neville MC (2002). Functional regulation of xanthine oxidoreductase expression and localization in the mouse mammary gland: evidence of a role in lipid secretion. *J Physiol* **545**, 567–579.

McManaman JL & Neville MC (2003). Mammary physiology and milk secretion. *Adv Drug Deliv Rev.* **55**, 629–641.

McManaman JL (2012). Milk lipid secretion: recent biomolecular aspects. *Biomol Concepts* **3**, 1–11.

Mroue R & Bissell MJ (2013). Three-dimensional cultures of mouse mammary epithelial cells. *Methods Mol Biol* **945**, 221–250.

Oftedal OT (2012). The evolution of milk secretion and its ancient origins. *Animal* **6**, 355–368.

Ogg SL, Weldon AK, Dobbie L, Smith AJ & Mather IH (2004). Expression of butyrophilin (Btn1a1) in lactating mammary gland is essential for the regulated secretion of milk-lipid droplets. *Proc Natl Acad Sci USA* **101**, 10084–10089.

Orlicky DJ, Monks J, Stefanski AL & McManaman JL (2013). Dynamics and molecular determinants of cytoplasmic lipid droplet clustering and dispersion. *PLoS One* **8**, e66837.

Ohtsubo T, Matsumura K, Sakagami K, Fujii K, Tsuruya K, Noguchi H, Rovira II, Finkel T & Iida M (2009). Xanthine oxidoreductase depletion induces renal interstitial fibrosis through aberrant lipid and purine accumulation in renal tubules. *Hypertension* **54**, 868–876.

Paoletti AC, Parmely TJ, Tomomori-Sato C, Sato S, Zhu D, Conaway RC, Weliky Conaway J, Florens L & Washburn MP (2006). Quantitative proteomic analysis of distinct mammalian Mediator complexes using normalized spectral abundance factors. *Proc Natl Acad Sci USA* **103**, 18928–18933.

Picariello G, Ferranti P, Mamone G, Klouckova I, Mechref Y, Novotny MV & Addeo F (2012). Gel-free shotgun proteomic analysis of human milk. *J Chromatogr A* **1227**, 219–33.

Robenek H, Hofnagel O, Buers I, Lorkowski S, Schnoor M, Robenek MJ, Heid H, Troyer D & Severs NJ (2006). Butyrophilin controls milk fat globule secretion. *Proc Natl Acad Sci USA* **103**, 10385–10390.

Russell TD, Palmer CA, Orlicky DJ, Fischer A, Rudolph MC, Neville MC & McManaman JL (2007). Cytoplasmic lipid droplet accumulation in developing mammary epithelial cells: roles of adipophilin and lipid metabolism. *J Lipid Res* **48**, 1463–1475.

Selbert S, Bentley DJ, Melton DW, Rannie D, Lourenço P, Watson CJ & Clarke AR (1998). Efficient BLG-Cre mediated gene deletion in the mammary gland. *Transgenic Res* **7**, 387–396.

Silanikove N, Shapiro F, Shamay A & Leitner G (2005). Role of xanthine oxidase, lactoperoxidase, and NO in the innate immune system of mammary secretion during active involution in dairy cows: manipulation with casein hydrolyzates. *Free Radic Biol Med* **38**, 1139–1151.

Sokac AM & Bement WM (2006). Kiss-and-coat and compartment mixing: coupling exocytosis to signal generation and local actin assembly. *Mol Biol Cell* **17**, 1495–1502.

Spertino S, Cipriani V, De Angelis C, Giuffrida MG, Marsano F & Cavaletto M (2012). Proteome profile and biological activity of caprine, bovine and human milk fat globules. *Mol Biosyst* **8**, 967–974.

Vizcaíno JA, Deutsch EW, Wang R, Csordas A, Reisinger F, Ríos D, Dianes JA, Sun Z, Farrah T, Bandeira N, Binz PA, Xenarios I, Eisenacher M, Mayer G, Gatto L, Campos A, Chalkley RJ, Kraus HJ, Albar JP, Martinez-Bartolomé S, Apweiler R, Omenn GS, Martens L, Jones AR & Hermjakob H (2014). ProteomeXchange provides globally co-ordinated proteomics data submission and dissemination. *Nature Biotechnol* **30**, 223–226.

Vorbach C, Scriven A & Capecchi MR (2002). The housekeeping gene xanthine oxidoreductase is necessary for milk fat droplet enveloping and secretion: gene sharing in the lactating mammary gland. *Genes Dev* **16**, 3223–3235.

Wagner KU, Wall RJ, St-Onge L, Gruss P, Wynshaw-Boris A, Garrett L, Li M, Furth PA & Hennighausen L (1997). Cre-mediated gene deletion in the mammary gland. *Nucleic Acids Res* **25**, 4323–4330.

Wagner KU, McAllister K, Ward T, Davis B, Wiseman R & Hennighausen L (2001). Spatial and temporal expression of the Cre gene under the control of the MMTV-LTR in different lines of transgenic mice. *Transgenic Res* **10**, 545–553.

Wang W, Lv N, Zhang S, Shui G, Qian H, Zhang J, Chen Y, Ye J, Xie Y, Shen Y, Wenk MR & Li P (2012). Cidea is an essential transcriptional coactivator regulating mammary gland secretion of milk lipids. *Nat Med* **18**, 235–243.

Wiśniewski JR, Zougman A, Nagaraj N & Mann M (2009). Universal sample preparation method for proteome analysis. *Nat Methods* **6**, 359–362.

Wooding FB, Peaker, M & Linzell, JL (1970). Theories of milk secretion: evidence from the electron microscopic examination of milk. *Nature* **226**, 762–764.

Wooding FBP & Sargeant TJ (2015). Immunocytochemical evidence for Golgi vesicle involvement in milk fat globule secretion. *J Histochem Cytochem* **63**, 943–951.

Wu CC, Howell KE, Neville MC, Yates JR 3rd & McManaman JL (2000). Proteomics reveal a link between the endoplasmic reticulum and lipid secretory mechanisms in mammary epithelial cells. *Electrophoresis* **21**, 3470–82.

Wu L, Zhou L, Chen C, Gong J, Xu L, Ye J, Li D & Li P (2014). Cidea controls lipid droplet fusion and lipid storage in brown and white adipose tissue. *Sci China Life Sci* **57**, 107–116.

Zeng R, Bequette BJ, Vinyard BT & Bannerman DD (2009). Determination of milk and blood concentrations of lipopolysaccharide-binding protein in cows with naturally acquired subclinical and clinical mastitis. *J Dairy Sci* **92**, 980–989.

## Additional information

### Competing interests

The authors declare no conflicts of interest.

### Contributions

JM conceived of and carried out the experiments, analysed the data, and wrote the paper. MD performed the mass spectroscopy and proteomic identification. ESB performed immunostaining. DJO performed histology and provided critical discussion. RMW provided the mice and contributed to the critical evaluation of the manuscript. JLM funded the work, provided critical discussion and edited the manuscript.

### Funding

National Institutes of Health: HL113809 to RMW, and 2R01HD45965 and 5P01HD038129 to JLM.

### Acknowledgements

This work is dedicated to the memory of Richard M. Wright. It would not have been possible without the resources provided by our colleagues, including Trevor Williams (Univ. Colorado Denver) and Kay-Uwe Wagner (Univ. Nebraska Medical Centre). The authors appreciate the contribution to this research made by E. Erin Smith, Allison Quador and Jessica Arnold of the University of Colorado Denver Histology Shared Resource. This resource is supported in part by the Cancer Centre Support Grant (P30CA046934). Additional technical support was provided by Radu Moldovon in the Advanced Light Microscopy Core and Dorothy Dill in the Electron Microscopy Core of the University of Colorado Anschutz Medical centre. The first author would like thank Ian Mather for helpful discussion, and Colin Monks for never-ending support. The work was supported by funding from the NIH. The funding sources had no role in study design, data collection or analysis, decision to publish, or preparation of the manuscript. The content is solely the responsibility of the authors.

## Supporting information

The following supporting information has available in the online version of this article.

Supplemental movies: XOR clusters Btn and remodels the glycocalyx (WGA).
Movies showing 3D reconstructions of docked and undocked CLD at the apical plasma membrane of WT and XOR MGKO mammary epithelial cells, respectively.
**Movie1.** Btn (red) and WGA (green) stained CLD from WT gland.
**Movie2.** Btn (red) and WGA (green) stained CLD from MGKO gland.
**Table S1.** NSAF values for all proteins identified in the proteomes of WT and XOR MGKO MFGs, in order of abundance. NSAF is calculated by dividing the total spectra counted for each protein, divided by the molecular weight of that protein, normalized to the total spectra counted

for that sample. Shown is the NSAF for WT and MGKO globules, the gene name, the common protein name, the accession number and the *P*-value.

**Table S2.** Changes in lipid metabolism proteins associated with the MFG of XOR MGKO dams. Proteins classified under the Gene Ontology term 'Lipid metabolism' present in all four samples of the XOR MGKO proteome in order of fold change from WT. Shown is the common protein name, the gene name, the NSAF and fold-change of MGKO/WT, as well as the *P*-value. Many proteins that are known to interact with one another show similar fold changes.